International Journal of Heat and Technology
Vol. 42, No. 1, February, 2024, pp. 219-237
Journal homepage: http://iieta.org/journals/ijht

A Review of BiOBr-Based Photocatalysts for Wastewater Treatment

Mohanad Mohmmed Mahdi[1,2*], Shahlaa Esmail Ebrahim[1]

[1] Environmental Engineering Department, College of Engineering, University of Baghdad, Baghdad 10001, Iraq
[2] Roads and Transport Engineering Department, College of Engineering, University of AlQadisiyah, Qadisiyah 58001, Iraq

Corresponding Author Email: mohanad.mohammed@qu.edu.iq

https://doi.org/10.18280/ijht.420123

Received: 30 December 2023
Revised: 24 January 2024
Accepted: 29 January 2024
Available online: 29 February 2024

Keywords:
wastewater treatment, photocatalytic process, BiOBr synthesis, BiOBr characteristics, BiOBr photo-degradation activity

ABSTRACT

Semiconductor based photo-catalysts which was an efficient process to treat water and wastewater. There are various techniques can be used for enhancement of photo-catalytic properties such as element rich strategy, defect control and facet engineering. Many methods were used for manufacturing of BiOBr, including ion-exchange method, solvothermal method, wet-chemical method, ultra-sonication method, co-precipitation method and hydrothermal method. Various operational parameters have such as initial pH of solution, catalyst dosage and inorganic ions have been employed to show their roles on the photo-degradation efficiency of pollutants. Elemental doping and coupled semiconductors are the widely using methods for enhancing BiOBr performance. It was concluded that the binary and ternary composites have the ability to enhancement the photo-catalytic activity and increased the degradation efficiency more than 50% compared with pure BiOBr. According to suitable band structure, bismuth bromide oxide is a promising candidate to treat wastewater efficiently by photo-catalytic technique.

1. INTRODUCTION

Industries and human activities have been responsible about air, water and land contaminations. Environment pollution particularly, water pollution has increased due to rapid increase in the population, which is a major threatens of the humanity existence [1, 2]. Wastewater or polluted water contains various pollutants such as organic, inorganic pollutants and pharmaceuticals [3-6]. Wastewater contaminated with dyes is highly hazardous for biological health and ecosystem, and the water bodies should be treating from these pollutants. In developing countries, waterborne pathogens such as bacteria and viruses were responsible for 80% of illnesses including giardiasis, diarrhea, typhoid fever, dysentery and salmonellosis [7]. It is necessary to kill these microorganisms and remove other pollutants to obtain drinking water [8]. However, various methods such as electrochemical reduction [9], membrane filtration [10-15], precipitation [16], electro-dialysis [17], photo-catalysis [18, 19] and electro-deionization [20] have been used for removing various pollutants and treatment of wastewater [11, 12]. The major disadvantages of these technologies except photo-catalysis are complicated process, large intake of energy, by-products formation and wastes, low removal efficiency and expensive so these technologies are not preferred in wastewater treatment. Photo-catalysis is an effective and green process, which is the best treatment process due to its cost-effectiveness and high efficiency; it has obtained the chemical energy from sunlight energy. Photocatalysis can be used in various applications like dye removal, microbial inactivation and eliminating pollutants from air, etc. [18].

By a series of reactions, photo-catalysis process has the ability to convert complex pollutants into very simple and harmless molecules. So, this technique has been an environment friendly and economically [21]. For current research and development, one of the common techniques for wastewater management is a nanotechnology [22].

Bismuth was discovered in the 1660s which is a white substance, it has an atomic mass of 208.98 [23-25]. Many important Bismuth ores are Bi_2S_3 and Bi_2O_3 [26]. Unlike many of heavy metals which are carcinogenic, highly toxic and cause fragility of bones, failure of kidney and lung damaging [27-32], bismuth is non-carcinogenic and non-toxic [33], bismuth is less toxic than table salt, which is regarded as a green element [27-29]. For long time, bismuth has been employed in several applications as pigments, cosmetics and medicines [30, 31], as well as using of bismuth vanadate in paints as a pigment [32]. In this aspect, many researches have been used bismuth in several applications as a replacement for toxic lead [34].

BiOBr has small band-gap (Eg=.64-2.91 eV) [35-37]; so, it has the ability for maximum visible sunlight energy harvesting photo-catalyst [38]. Bismuth is non-toxic and chemically stable as well as cheap [39-41]. There are several shapes of BiOBr, including nanoflowers [42], nanobelts [43] and nanoflakes [44] and nanospheres [45] which have been manufactured by several methods like solvothermal [43], hydrothermal [46], ion thermal [47], and co-precipitation [48]. Now, bismuth is being used for various purposes, such as photo-catalytic wastewater treatment [49], water splitting [42], indoor-gas purification [50] and alcohol selective oxidation [51].

Bismuth bromide oxide belongs to BiOX (X=I, Br, Cl, F)

family, which crystallizes with layered tetragonal matlockite structures [52]. BiOX compounds are characterize good magnetic and electrical properties, which have been used in various field such as photo-chromic devices, solar cells, ferr-oelectric materials and pigments [53, 54].

In each layer, four atoms of halogen surround the bismuth center (having weak interlayered interactions) and four atoms of oxygen (having strong covalent bonds) [55], as shown in Figure 1.

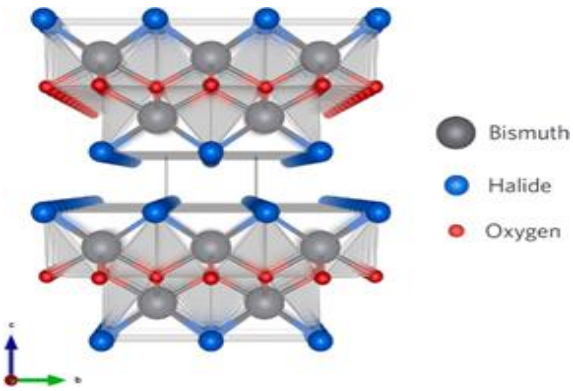

Figure 1. BiOX (X = I, Br, Cl, F) crystal structure systems [56]

For improving the overall degradation process, another form of composites has been used which are called ternary composites. The advantages of ternary composites are to suppress the recombination of photo-induced charges and provide more active sites than binary composites [57-61].

The aims of this study are reviewing recent works on the BiOBr synthesis methods, the characteristics of fabricated BiOBr, the pristine BiOBr photo-catalytic activity and operating parameters affecting on the degradation process using BiOBr composite.

2. SEMICONDUCTOR PHOTO-CATALYSIS

Semiconductor is a material has conductivity between conductors and insulators. Semiconductor photo-catalysis are a photo-chemical reaction whereby a quantum of light (visible, ultraviolet or infrared radiation) was absorbed by a semiconductor for initiate a chemical reaction [62]. Photo-catalytic is a heterogeneous process, which uses different semiconductors like oxides (ZnO, CeO_2, TiO_2, WO_3, ZrO_2, Fe_2O_3, etc.) and sulfides (ZnS, CdS, etc.) in the presence of visible light [63-65]. Titanium dioxide (TiO_2) is characterized as low energy consumption, photo and chemical stability, high photo-catalytic activity, ease of available, low operation temperature and nontoxic byproducts formation [66-69]. The basic elements should be provided for completing of a photo-catalytic reaction are: a photo-catalyst, source of light and the transformation of the chemical reaction partners. A semiconductor photo-catalyst must be photo-active and photo-stable, biologic and chemical inert, inexpensive and ecologic friendly to promote its functions [70].

The photocatalytic activity of semiconductors has been affected by several parameters such as phase structures, crystalline, particles size, defects and composition. It was reported the influence of these factors on the ZnO activity [71]. There is difference in the photocatalytic activity at various values of specific surface area of rods: 8.02, 7.85, 7.91, and 6.04 m^2/g. It was noticed that the improving of photogenerated carriers separation was related to the structure and aspect ratio of the facets. Thus recombination centers were decreased leading to higher photocatalytic efficiency [72, 73].

BiOBr is characterized as narrow-band gap Semiconductor [74] which is more suitable than other photo-catalysts such as ZrO_2, TiO_2, ZnO and SnO because it has the ability for absorbing the maximum portion of visible sunlight due to narrow band gap. When a photo-catalyst is irradiated by light of the desired wavelength, the electrons-holes were transferred to the semiconductor surface and may recombine. This recombination has been producing heat and phonons, the number of charge carries have been decreased and affect the photo-catalysis efficiency. So, binary and ternary composites like BiOI/BiOBr [35], GQDs/BiOBr [75] and BiOBr/W18O49/PAN [76] have been developed to enhance the photo-catalysis efficiency.

In a photo-catalytic reaction, the electrons excited from VB of the particular semiconductor to CB by providing sufficient and enough amount of photons energy (hυ). The region of empty energy between these bands is called band-gap (Eg) [77]. The positions of VB and CB are essential features for determining the photo-catalytic ability of a semiconductor [78].

Generally, by irradiation of a semiconductor photo-catalyst with photons energy greater than its band-gap, this led to a photo-catalytic reaction gets initiated. The oxidative species that are generated in a photo-catalytic reaction is shown in Figure 2.

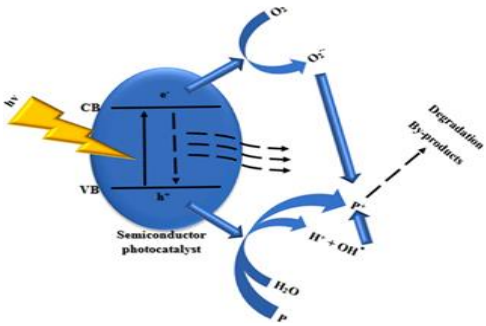

Figure 2. Schematic illustration of a typical photo-catalytic reaction [79]

In the conduction band, molecular oxygen (O_2) adsorbed has the ability to trap the electron (e^-_{CB}), which is reduced to form superoxide radical anion ($O_2^{\bullet-}$). Subsequently, ($O_2^{\bullet-}$) radical can be further protonated to form hydro-peroxyl radicals ($HOO^\bullet$), then formation of hydrogen peroxide (H_2O_2) [80]. The generated ($O_2^{\bullet-}$) and ($HOO^\bullet$) have the ability for degradation of organic pollutants (P) directly. On the other hand, the holes are capable of either producing intermediate products by directly oxidizing P or producing hydroxyl radicals ($OH^\bullet$) by oxidizing H_2O. Eqs. (1)-(10) below show a photo-catalytic reaction mechanism [81]:

$$\text{BiOBr photo-catalyst} + hv \rightarrow e^- + h^+ \quad (1)$$

$$e^- + O_2 \rightarrow O_2^{\bullet-} \quad (2)$$

$$h^+ + H_2O \rightarrow H^+ + OH^\bullet \quad (3)$$

$$h^+ + OH^- \rightarrow OH^\bullet \quad (4)$$

$$O_2^{\bullet-} + H^+ \rightarrow HOO^\bullet \quad (5)$$

$$HO_2^{\bullet} + HO_2^{\bullet} \rightarrow H_2O_2 + O_2 \quad (6)$$

$$h^+ + P \rightarrow \text{intermediate products} \rightarrow CO_2 + H_2O \quad (7)$$

$$O_2^{\bullet -} + P \rightarrow \text{intermediate products} \rightarrow CO_2 + H_2O \quad (8)$$

$$OH^{\bullet} + P \rightarrow \text{intermediate products} \rightarrow CO_2 + H_2O \quad (9)$$

$$HOO^{\bullet} + P \rightarrow \text{intermediate products} \rightarrow CO_2 + H_2O \quad (10)$$

3. SYNTHESIS OF BIOBR COMPOSITES

The photo-catalytic efficiency of composites can be enhanced by coupling of two or more semiconductors due to enhancing the surface area as well as synergistic role of each semiconductor. Various factors that influence the morphology, size, and properties of BiOBr composites such as pH and temperature. It was found that at pH equal to 8, best BiOBr photocatalytic activity has been obtained for photodegradation of rhodamine B. [82]. Temperature parameter has important effect on the size, and properties of BiOBr composites. At increasing the value of temperature, the BiOBr activity was increased and then decreased due to has a good crystallization. While for BiOCl, the efficiency was decreased due to decreasing in specific surface area and pore size [83].

BiOBr composites have been manufactured mainly by several processes such as: Ion exchange [84], solvothermal [85], wet chemical [86] ultra-sonication [87], co-precipitation [88] and hydrothermal methods [89].

3.1 Ion-exchange method

This method includes formed a new product by using a desired chemical species instead of present ionic species. For instance, using ion exchange method for synthesize of Bi/BiOBr/AgBr. Firstly, Bi/BiOBr were fabricated by dissolving sodium bromide (0.001 mol) in 30 ml of ethylene glycol and heated at 180℃ for 15 h in Teflon-lined autoclave. Then, the synthesized particles were separated by centrifugation, washed with pure water/absolute ethanol for many times and dried for 4h at 80℃. After that, it was used ion exchange method to synthesize of Bi/BiOBr/AgBr. In which, 0.001 mol of $AgNO_3$ was dissolved in 80 mL ethylene glycol (80 mL), then added of synthesized Bi/BiOBr microspheres (0.4 g) to the mixture and stirred for 12h. Then, the synthesized particles were separated by centrifugation, washed three times and dried at 80℃ for 4 h [84].

Figure 3 shows the Bi/BiOBr, BiOBr/AgBr and Bi/BiOBr/AgBr phase structures were characterized by XRD [90-92].

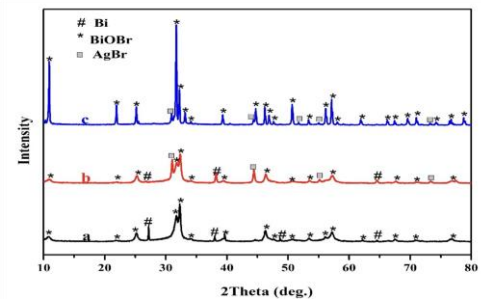

Figure 3. XRD patterns of (a) Bi/BiOBr; (b) Bi/BiOBr/AgBr and (c) BiOBr/AgBr

3.2 Solvothermal method

A Teflon-lined autoclave was used for heating the precursors. To produce precursor solutions, a variety of the solvents are used such as ethanol [93], ethylene glycol [94] and glycerol [95]. For instance, the solvothermal route has been used to synthesis CdS/BiOBr binary composites. Firstly, CdS has been synthesized by dissolving (2.666 g) of $C_4H_6CdO_4{\cdot}2H_2O$ and (2.256 g) of CH_3CSNH_2 in de-ionized water (30 mL) and stirring for 1 h. During stirring, CH3CSNH2 solution was added into the cadmium nitrate solution. Then, the mixture was heated at 120℃ for 24 h in Teflon-lined autoclave. The synthesized particles were separated by centrifugation, washed with pure water/absolute ethanol for three times and dried for 6 h at 60℃.

To synthesize of BiOBr, (1.0902 g) of bismuth nitrate was dissolved in 30 mL of ethyl glycol and mixed with 0.078 M of KBr. Then, a Polyvinylpyrrolidone (0.3020 g) was added into the $Bi(NO_3)_2 \cdot 5H_2O$ and stirred for 30 min. After that, 0.078 M KBr solution was added to the mixture under stirring for 1 h. Then, the mixture was heated at 160℃ for 12 h in Teflon-lined autoclave. The synthesized particles were separated and washed with pure water/absolute ethanol for many times and dried for 6h at 60℃.

Finally, to synthesize of CdS/BiOBr binary composites, take (0.3033 g) of synthesized CdS and added to 0.07 M of KBr solution. Then, a Polyvinylpyrrolidone (0.3207 g) was added into 0.0868 M of $Bi(NO_3)_3 \cdot 5H_2O$. Separately, both mixtures were separately stirred for 1 h. After that, the suspension of CdS and KBr was added into the bismuth nitrate solution with stirring for 1 h. The synthesized particles were separated and washed with pure water/absolute ethanol for many times and dried for 6h at 60℃ [96]. By using solvo-thermal method, there are various BiOBr based composites can be synthesized like BiOCl/BiOBr [97], PANI/BiOBr/$ZnFe_2O_4$ [98] and Fe_3O_4/mSiO_2/BiOBr [95].

Also, the BiOBr physicochemical properties were influenced by the initial reaction pH value. For instance, synthesizing of BiOBr catalysts with different values of reaction pH. It was noticed that the average thickness and width of BiOBr nanosheets were inversely proportional with pH value, as shown in Table 1, even though the basic samples units were nanosheets, see Figure 4 [99].

Table 1. BiOBr sizes and specific surface areas at various pH [99]

pH Value	Width (μm)	Thickness (nm)	S_{BET} (m^2/g)
1	2-4	110-130	2.51
3	1-3	80-90	5.18
5	1-2	60-80	5.80
7	0.5-2	40-60	11.91

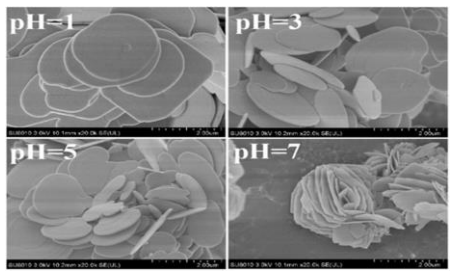

Figure 4. FE-SEM of BiOBr samples at various values of pH [99]

Moreover, with the high value of pH, the (001), (002), (003) and (004) diffraction peaks (shown in Figure 5) weakened due to the reduced exposure percentage of [001] facets. Also, it was concluded that BiOBr has been nucleation at pH value was increased leads to a decrease in crystallite size, so the BET specific surface area is directly proportional to the pH value, see Table 1.

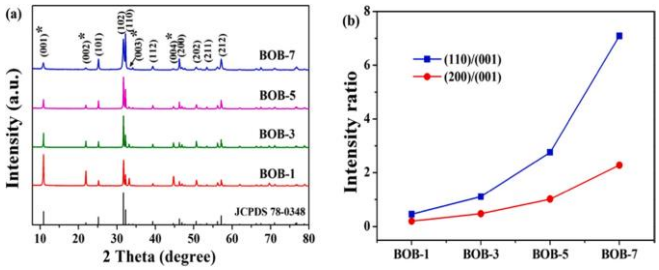

Figure 5. (a) BiOBr XRD patterns and (b) their peak intensity ratios of BiOBr samples [99]

3.3 Wet-chemical method

In this method, it was synthesized of composites in suitable liquid such as deionized water. For instance, Gao et al. fabricated of $BiPO_4$/BiOBr binary composites by using wet-chemical method. In which, 0.01 mol of synthesized BiOBr was dissolved in ethanol (40 mL). Then, it was added the concentrated H_3PO_4 to the solution with and stirred for 20 min. The obtained particles were washed and dried at 80 C for 12 h to obtain $BiPO_4$/BiOBr composites [100]. The BiOBr phase structures and $BiPO_4$/BiOBr were characterized by XRD, and the results are shown in Figure 6.

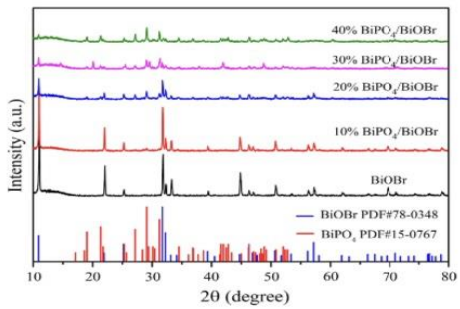

Figure 6. XRD patterns of BiOBr and BiPO4/BiOBr [100]

3.4 Ultra-sonication method

Ultrasonic processing has been used to process the mixtures of reaction for a suitable time. For example, Cheng et al. [101] used this method for synthesizing of BiOBr/$Bi_2O_2CO_3$ binary composite. Firstly, $Bi_2O_2CO_3$ was synthesized by dissolving 1.4553 g of Bi $(NO_3)_3$•$5H_2O$ in 60 mL of diluted HNO_3. Then, it was added a urea (3.6 g) to the solution and sonication treated for 10 min. The solution was heated at 160℃ for 10h in a Teflon-lined autoclave. The produced particles were washed and dried at 80℃.

To synthesize of BiOBr, 1.4553 g of Bi $(NO_3)_3.5H_2O$ was dissolved in 30 mL of pure water and treated ultra-sonically for 20 min. On the other hand, 0.309 g of sodium bromide was dissolved in 30 mL of pure water and dropped this solution to the above solution and treated the mixture ultra-sonically for 10 min. The solution was heated at 160℃ for 10h in a Teflon-lined autoclave. The produced particles were washed and dried at 80℃.

Finally, to synthesize of BiOBr/$Bi_2O_2CO_3$ binary composites, 0.515g sodium bromide was dissolved into 50 mL of pure water. Then, 0.5 g of synthesized $Bi_2O_2CO_3$ was dispersed in the above solution and treated the mixture ultra-sonically for 40 min. The produced particles were washed with water and dried at 80℃ [101].

3.5 Co-precipitation method

This method required less time and low temperature, which is environment friendly as compared to other methods.

Zhao et al. [102] used this method for synthesizing of BiOBr/TiO_2 composite. In which, during an appropriate amount of potassium bromide has been dissolved into 20 mL of de-ionized water, an appropriate amount of Bi $(NO_3)_3.5H_2O$ was added into de-ionized water (20 ML) to form suspension X_1. After that, TiO_2 nanobelts (40 mg) were dispersed in to potassium bromide with stirring to form suspension X_2. After that, the suspension X_2 was added slowly into the suspension X_2 under stirring at room temperature for 30 min. Then, the synthesized particles were separated and washed with pure water/ethanol solution and dried at 60℃ to form BiOBr@TiO_2 hetero-structures.

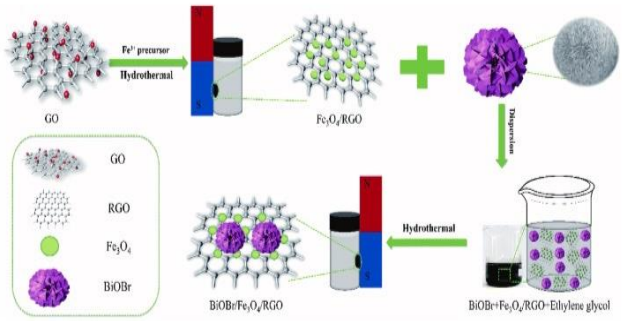

Figure 7. Mechanism of using PANI/BiOBr/$ZnFe_2O_4$ for photo-catalytic degradation of nitrobenzene [59]

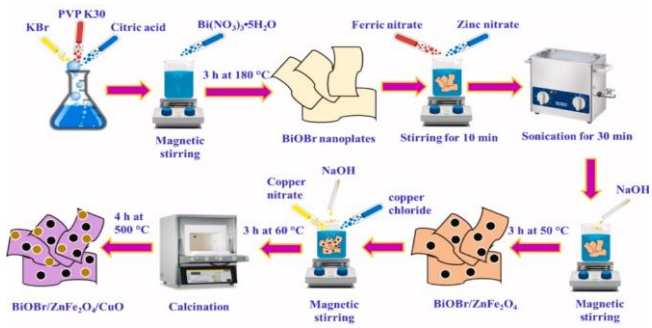

Figure 8. Schematic illustration explains of the constructing of BiOBr/$ZnFe_2O_4$/CuO nano composites [103]

3.6 Hydrothermal method

Water has been used as a solvent in hydrothermal method. For instance, Jiang Y. et al. used this method for fabricating BiOBr/BiOI binary composites for the photo-catalytic crystal violet dyes degradation. The general procedure includes adding of precursors into water/nitric acid and transfer the mixture to an autoclave and heat at (110-260℃) for 12 h. Then,

a variety of hetero-structures are produced [89]. Moreover, this method has been used for synthesizing of Ternary composites of $BiOBr/Fe_3O_4/rGO$ [60], as explain in Figure 7. Also, Figure 8 shows the fabricating $BiOBr/ZnFe_2O_4/CuO$ photo-catalyst by a hydrothermal method [102]. The phase structures of BiOBr, $ZnFe_2O_4$, CuO, and $BiOBr/ZnFe_2O_4/CuO$. were characterized by XRD [103], see Figure 9.

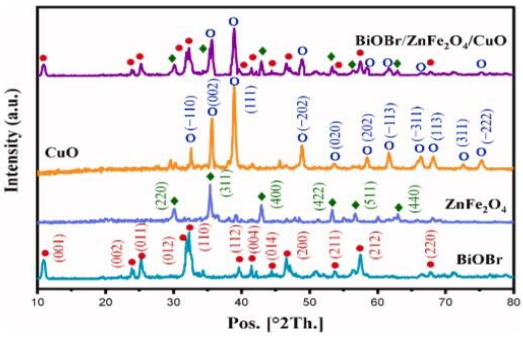

Figure 9. XRD patterns of BiOBr, $ZnFe_2O_4$, CuO, and $BiOBr/ZnFe_2O_4/CuO$ [103]

4. APPLICATION OF BIOBR IN WASTEWATER TREATMENT

In the photocatalytic process, the photo-catalyst was interacted to the incident visible light for creating the electron-hole (e^- / h^+) pairs [104, 105]. The visible light has the ability to promoted the valence band electron to the conduction band, while a hole (h_{VB}^+) is generated by the interaction of visible-light. These charges have the ability for reacting with adsorbed species and migrate from the bulk to the surface of photocatalysis [106, 107].

Binary and ternary composites have the ability to enhancement the photo-catalytic activity and increased the degradation efficiency more than 50%. For example, Han et al. [108] showed that the chlorophenol degradation was increased from 0.8% (by using BiOBr composite) to more than 92% (by using $BiOBr/NaBiO_3$). Band structure, band gap and interface of the composites have the ability for enhancement of photo-catalytic efficiency. Formation of narrow binary composite band gap is the main factor for enhancement the photo-catalytic activity by increased sunlight harvesting, it was shown that the BiOBr and $NaBiO_3$ band gabs are 2.880 eV and 2.60 eV, respectively, which was reduced to 2.52 eV when the formation of $BiOBr/NaBiO_3$ binary composite. Conclusively, efficient visible light harvesting resulted in binary composite due to modulated band gap.

Although the binary composites have the ability for enhancing the photo-catalytic activity, but still not perfect in practical applications. So, researchers have been increased charge separation and enhanced surface area by synthesizing of ternary composites. For example, in the case of Bi/BiOBr/AgBr composites, the degradation percentage of wastewater pollutants was increased from 48% (BiOBr) to more than 95%. Furthermore, metal-oxygen bond has the ability to recovery of composites after pollutants degradation and has the ability for increasing surface area, like $BiOBr/Fe_3O_4/RGO$ [60], $Fe_3O_4/BiOBr/BiOI$ [94], $Fe_3O_4/mSiO_2/BiOBr$ [95] and $Fe_3O_4/BiOBr/CQDs$ [109]. Conclusively, ternary composites have more adsorption area for pollutants and more ability for degrading pollutants than binary composites, for example, the rhodamine B degradation efficiency by Bi/BiOBr/AgBr was 4.9 and 1.4 times faster than BiOBr/AgBr and Bi/BiOBr, respectively [84]. Similarly, $BiOBr/TiO_2/G$ has the ability for degradation of various wastewater pollutants more efficiently than $BiOBr/TiO_2$ [89, 110-113] and the degradation efficiency of g-C_3N_4/BiOI/BiOBr was a better than BiOI/BiOBr [102, 114-118]. Also, $Bi_2O_2CO_3/Ti_3C_2T_x$ heterostructure has the ability to degrad 95.4% of levofloxacin, while the degradation efficiency was 68.1% by using $Bi_2O_2CO_3$ [119].

Several operating parameters like dose of a semiconductor, pollutants concentration and intensity of visible light irradiation have been studied in the literature. Higher catalyst concentrations provide reactive radical's generation. On the other hand, due to particles aggregation, the effective path-length of radiation was reduced when using excess of catalyst [120-122].

5. PHOTO-CATALYTIC ACTIVITY OF BIOBR

The previous studies indicated that the treatment of water contaminated with synthetic dyes become difficult due to stability of dyes in water. Recently, nanoparticles under visible light have the ability for removing dyes from wastewater [22]. Various organic pollutants were degraded by using BiOBr as catalyst with visible light. However, the hierarchical structure, surface area, crystallization are the main factors that affecting the degradation efficiency of pollutants. For instance, Xia et al. [123] used BiOBr nanospheres for degrading of 10 mg/L of (RhB), it was found that the degradation percentage was 100% when using BiOBr nanospheres as catalysts. While, the degradation percentage was 75% after 105 min by using hollow spheres.

Xue et al. [124] used 3D-BiOBr hierarchical microspheres for degrading 7 mg/L of Rhodamine Blue (RhB) by using 1:1, 1:2 and 2:1 molar ratios of Br:Bi for 35 min detention time, it was found that the degradation efficiencies were 91.1%, 88.6% and 95.9%, respectively. Due to high percent of Bi compared with Br in the second mixture, the degradation efficiency as low compared with other efficiencies.

BiOBr photo-catalytic activity was also found to be impacted by its hydrothermal pH value. For instance, Ye et al. [125] used BiOBr with three different values of pH (0.4, 6 and 10) for degradation of 10 ppm of RhB. It was found that the degradation efficiencies after 2h were 67%, 83% and 99%, respectively. It was concluded that the BiOBr photo-catalytic activity has a direct relationship with pH value because the BiOBr band structure, size and its surface area are affected by its hydrothermal pH value.

By comparing the BiOBr activity with other commonly used photocatalysts, the Rhodamine (RhB) degradation efficiency was 92% by using Ni-ZnS/g-C_3N_4 heterojunction after 75 min [126]. Another study showed that by using Iron oxide/CdS to degrade Xylenol blue (XB), the photodegradation efficiency was 90.2% after 3 hr [127]. Also, it was reported that the $BiOBr/ZnFe_2O_4/CuO$ photocatalyst has optimum photocatalytic properties, which has the ability for destroying 98% of malachite green in 90 min [103].

Band-gap, mesoporous structure, surface area and synergistic effect between TiO_2 and BiOBr are the main factors that affect the photocatalytic activity of BiOBr nanoparticles such as band-gap, mesoporous structure, surface area and synergistic effect between TiO_2 and BiOBr [128].

6. ENHANCING THE PHOTO-CATALYTIC PERFORMANCE OF BIOBR

The electron-hole recombination is an important process in semiconductors due to it plays a crucial role in photocatalytic reactions [129]. The electron-hole recombination cause losses in copper zinc tin sulfide charge and energy [130].

To enhance the BiOBr performance, there are many efforts and methods have been used for this purpose. The widely used methods are discussed below.

6.1 Elemental doping

Several dopants have been used to enhance the photo-catalytic activity of BiOBr, as tabulated in Table 2.The most important efforts include inhibits recombination of electron-hole by doping an appropriate number of cations [131]. Some of the cations can be introduced to improve other properties, such as redox-potential of the photogenerated radicals and the ability of BiOBr for harvesting of visible light [132]. However, it was noted that photo-catalytic activity was decreased in the presence of excess cationic dopants because these dopants serve as recombination centers [133].

To inhibit the electron- hole recombination, it was used Ag–TiO_2−xNx to separate of electrons and holes under UV-visile light. The higher efficiency of this composite is reacted to the electrons and holes density. So, the Ag loading has the ability for decreasing of the recombination and enhancing the photocatalytic activity. The electron acceptors can be inhibit the fast electron-hole recombination by accelerating the electron transfer [134, 135].

Many researchers studied the BiOBr photo-catalytic activity loaded with noble metals. For instance, using photo-deposition method for loading palladium nanoparticles onto the surface of BiOBr. It has been further loading of palladium nanoparticles onto BiOBr surface for enhancing the Pd-doped BiOBr absorbance intensity. The phenol degradation was 67% only by using BiOBr for 5h. While, when using 0.5 Pd-BiOBr, it was successfully degraded all phenol [136]. Moreover, using photo-reduction method for dispersing Pd NPs onto BiOBr surface [137].

Other forms of cationic dopants are the transition metals that were reportedly introduced into BiOBr, this method has the ability for improving the absorbance intensity in the visible region as well as inhibit recombination of electron-hole. For instance, synthesizing of Fe-doped BiOBr photo-catalysts for methyl orange degradation, it was noticed that the photo-catalytic activity of Fe-doped BiOBr more effective than that of pristine BiOBr [131]. Similarity, synthesizing of Zn-doped BiOBr catalysts with a 300 W Xe lamp to degrade RhB dye [133]. Many authors studied the potential for leaching of dopants, it was reported that the catalytic site of combined W dopants and Co vacancies was less active than the W dopants alone. However, the leaching-induced Co vacancies with residual W dopants cause decreasing of current density and the created cataytic sites is more active than generated by W dopants alone. As a result, the photocataytic activity of combined W dopants and Co vacancies has been enhanced [138].

Literature has also used the anionic dopants onto BiOBr surface to inhibits recombination of electron-hole. For instance, B-doped BiOBr samples was synthesized for the RhB dye degradation. It was reported high degradation efficiency of B-doped BiOBr compared with alone pristine BiOBr [139]. Also, degradation of RhB dye by S-doped BiOBr. It was found that the degradation rate of S-doped BiOBr was 0.0960 per min. While, it was 0.0176 per min of pristine BiOBr [140].

Table 2. The photo-degradation efficiencies of common BiOBr and doped BiOBr catalysts

Dopant	Source of Light	Experimental Conditions [Pollutant]; Dosage; Time of Irradiation	Photo-Degradation Efficiency, %		Reference
			BiOBr	Doped BiOBr	
Er	300 W Xe lamp with a light cut-off filter (λ>400 nm)	CIP]=10 mg/L; 100 mg/L; 360 min	50	61	[132]
Ag	500 W Xe lamp	[MO]=10 mg/L; 200 mg/L; 120 min	58.5	98.6	[137]
Fe	150 W halogen-lamp with light intensity of 200 mW/ cm^2	[MO]=10 mg/L; 1000 mg/L; 120 min	75	100	[131]
Ti	11 W lamp with a light cut-off filter (λ≥400 nm)	[RhB]=10 mg/L; 1000 mg/L; 180 min	-75	100	[141]
Pt	300 W Xe lamp to provide visible light (320 nm<λ<680 nm)	[PNP]=10 mg/L; 1000 mg/L; 30 min	-25	100	[52]
Cu	200 W Xe arc lamp with a light cut-off filter (λ≥420 nm)	[NOR]=10 mg/L; 1000 mg/L; 90 min	-20	-45	[142]
Cu	200 W Xe arc lamp with a light cut-off filter (λ≥420 nm)	[NOR]=10 mg/L; 1000 mg/L; 90 min	-20	-45	[142]
Co	Xe lamp (500 W) with a light cut-off filters (λ≥400 nm)	[RhB]=10 mg/L; 1000 mg/L; 120 min	34	99.5	[143]
Mn	Daylight lamp with a light cut-off filters (λ≥400 nm)	[RhB]=0.2 g/L; 1000 mg/L; 140 min	78	96.5	[144]
Nb	300 W Xe lamp with a light cut-off filters (λ≥420 nm)	[RhB]=10 mg/L; 200 mg/L; 20 min	51	-100	[145]
S	11 W lamp with a light cut-off filter (λ≥400 nm)	[RhB]=10 mg/L; 400 mg/L; 60 min	-45	-100	[146]
I[a]	500 W Xe lamp with a light cut-off filter to provide visible light (λ=400 nm)	[MO]=10 mg/L; 2000 mg/L; 180 min	-20	-70	[147]
S	1000 W Xe lamp with a UV cut-off filter (λ≥420 nm)	[RhB]=20 mg/L; 500 mg/L; 50 min	50	100	[140]
Bi	300 W perfect Xe lamp with a UV cut-off filters	[TC]=NA;	-30	-100	[148]

	(λ≥400 nm)	800 mg/L; 20 min			
B	150 W tungsten lamp with a UV cut-off filters (λ≥420 nm)	[RhB]=15 mg/L; 1000 mg/L; 30 min	71.1	99.3	[139]
Y	25W Eco-living day light fluorescent	[CIP]=20 mg/L; 1000 mg/L; 60 min	71.7	87.6	[149]

*CIP = Ciprofloxacin; RhB = Rhodamine B; MO = Methyl Orange; TC = Tetracycline; PNP = p-nitro- phenol; NA = Not Available; W = Watts.

6.2 Coupled semiconductors

The formation of hetero-junction with semiconductors is another widely approach has been used for improving the photo-catalytic performance of photocatalysts [150].

The synergistic effects on the photo-catalytic performance have been studied. It was reported synergetic effect on g-C_3N_4 structure, the g-C_3N_4 has the ability to create gap states. while the g-C_3N_4 band edge can be tune by coupling effect at g-C_3N_4/MoS_2 interface, this modification has the ability for inhibiting the electron-hole recombination by affecting the electron distribution [151].

Metal-organic frameworks (MOFs) have several properties make it more suitable for photocatalytic applications, but there stability is the most important challenge, the stability of these compounds is limited. To overcome these limitations, many authors developed composite materials such as utilizing molybdenum disulfide (MoS_2), in combination with (MOFs). It was concluded that the MoS_2/MOF heterojunctions were high photochemical stability and effective compared to pure MOFs due to there. It was indicated that these composites have the ability for using in practical applications [152].

such as tabulated in Table 3. Bismuth-based semiconductors are the most common coupling semiconductors have been used in photocatalytic process. For example, Qiu et al. [153] used solvothermal method for loading different amounts of bismuth sub-carbonate ($Bi_2O_2CO_3$) onto BiOBr nanosheets to form $Bi_2O_2CO_3$/BiOBr (BOC/BOB). The degradation efficiency of fabricated $Bi_2O_2CO_3$/BiOBr p-n heterojunction composites was a better than pristine BiOBr or pristine $Bi_2O_2CO_3$ degradation efficiencies under visible light. There are many factors which enhanced the performance of composites, including: the p-n hetero-junction, suppressed recombination and facilitating charge separation. Also, Su and Wu [154] used hydrothermal method to construction of BiOBr/$Bi_4O_5Br_2$ composites for photo-catalytic degradation of CIP at various pH (pH=4, 5, 6 and 7). It was noticed that the highest degradation efficiency can be obtained by synthesized of the BiOBr/$Bi_4O_5Br_2$ composite at pH 7.

Another widely approach is loading metal-free carbonaceous materials, like carbon quantum dots (CQDs) on to BiOBr. For example, Xia et al. [155] used different weight ratio of CQD to BiOBr for synthesizing a series of CQDs/BiOBr to degrade of RhB dye. It was noticed that the pristine BiOBr degradation efficiency was 37% only after 30 min. While, the degradation efficiency of CQDs/BiOBr was 100%, as shown in Figure 10.

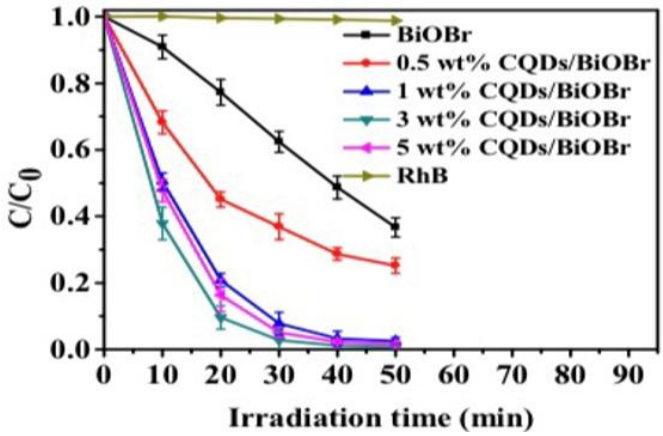

Figure 10. The photo-catalytic degradation of RhB in the presence of 1CQDs/BiOCl composites [155]

Table 3. The photo-degradation efficiencies of common BiOBr and coupled BiOBr catalysts

Coupling Catalyst	Source of Light	Experimental Conditions Dosage; [Pollutant]; Time of Irradiation	Photo-Degradation Efficiency, (%)		Reference
			Pristine BiOBr	Coupled BiOBr	
$Bi_4O_5Br_2$	Improvised photo-catalysis reactor under 500 W Xe lamp	[CIP] = 10 mg/L; 1000 mg/L; 150 min	50	91	[154]
$Bi_2O_2CO_3$	500 W Xe lamp (λ > 420 nm)	[RhB] = 10 mg/L; 500 mmg/L; 45 min	46.99	92.83	[156]
CdS	1 kW Xe lamp	[MG] = 15 mg/L; 600 mg/L; 100 min	~ 20	99	[157]
$NiFe_2O_4$	350 W Xe lamp (λ > 420 nm)	[MB] = 10 mg/L; 1000 mg/L; 60 min	45	90	[158]
$CoTiO_3$	Xe lamp (500 W)	[RhB] = 10 mg/L; 1000 mg/L; 50 min	~ 40	100	[159]
CQDs	Xe lamp (500 W) equipped with a light filter (λ = 420 nm)	[RhB] = 10 mg/L; 300 mg/L; 20 min	67	92	[157]
ZnO	Xe lamp (300 W) equipped with a light filter (λ = 420 nm)	[RhB] = 5 mg/L; 1000 mg/L; 130 min	58	95	[160]
$CoFe_2O_4$	Xe lamp (300 W) as a simulated solar light source	[CR] = 15 mg/L; 1000 mg/L; 60 min	62.27	90.78	[161]
CQDs	Xe lamp (300 W) equipped with a light filter (λ = 400 nm)	[RhB] = 10 mg/L; 200 mg/L; 30 min	37	~ 100	[155]
TiO_2	104 W Slovenia cool white lamp	[CIP] = 25 mg/L;	30.7	95.5	[162]

	(λ = 390–700 nm)	1000 mg/L; 180 min			
WS_2	Xe lamp (500 W) to obtain visible light with a UV cut-off filter (λ > 400 nm)	[CIP] = 20 mg/L; 1000 mg/L; 100 min	61	92	[163]
FePc	Xe lamp 350 W equipped with a UV filter (λ ≥ 400 nm)	[CIP] = 10 mg/L; 400 mg/L; 4 h	~ 30	~ 60	[164]
g-C_3N_4	Xe lamp 300 W equipped with a UV cut-off filter (λ ≥ 400 nm)	[CIP] = 10 mg/L; 200 mg/L; 6 h	67	85	[165]
WO_3	500 W Xe lamp equipped with a UV cut-off filter (λ ≥ 400 nm)	[CIP] = 20 mg/L; 500 mg/L; 120 min	59.1	94.7	[166]
α – Fe_2O_3	300 W Xe lamp equipped with a UV cut-off filter (λ ≥ 420 nm)	[RhB] = 20 mg/L; 1000 mg/L; 40 min	60	95	[167]
C3N4	300 W Xe lamp with two cut-off filters (λ = 320–780 nm)	[RhB] = 20 mg/L; 500 mg/L; 40 min	~ 65	100	[168]
BHO	300 W Xe arc lamp equipped with a 385–740 nm desired filters	[RhB] = 15 mg/L; 500 mg/L; 50 min	~ 75	100	[169]
CdS	Halide lamp (250 W) with a light cut-off filter (λ ≥ 400 nm)	[RhB] = 20 mg/L; 1000 mg/L; 50 min	74	97	[170]
Bi_2O_4	I300C Xe lamp	[MO] = 20 mg/L; 1000 mg/L; 10 min	~ 15	100	[171]
$CdWO_4$	Xe lamp (300 W) equipped with a UV cut-off filter (λ ≥ 420 nm)	[RhB] = 10 mg/L; 500 mg/L; 8 min	40	~ 100	[172]
TiO_2	Xenon arc lamp (300 W) equipped with a UV cut-off filter (λ ≥ 400 nm)	[MO] = 10 mg/L; 1000 mg/L; 80 min	~ 40	~ 91	[173]
$BiSbO_4$	Xe lamp (300 W) equipped with a UV cut-off filter (λ ≥ 400 nm)	[RhB] = 10 mg/L; 300 mg/L; 45 min	30	96	[174]
Graphene	xenon lamp (500 W) equipped with a UV cut-off filter (λ ≥ 400 nm)	[RhB] = 10 mg/L; 200 mg/L; 24 min	50	100	[175]
BiOCl	LED light irradiation	[MB] = 10 mg/L; 1000 mg/L; 360 min	72	93	[176]
TiO_2	300 W xenon lamp equipped with a UV cut-off filter (λ ≥ 400 nm)	[RhB] = 10 mg/L; 250 mg/L; 40 min	~ 70	~ 100	[177]
Bi_2MoO_6	50 W LED light (410 nm)	[MB] = 20 mg/L; 1000 mg/L; 40 min	> 20	> 90	[178]
QDs-Cu_2O	250 W halide lamp with equipped with a UV cut-off filter (λ ≥ 400 nm)	[MB] = 10 mg/L; 1000 mg/L; 60 min	73	95	[179]
$FeWO_4$	Xe lamp (300 W) with a 400 nm cut-off filter	1000 mg/L; 60 min	66.2	90.4	[180]
$LaFeO_3$	200 W Xe lamp emitting simulated sunlight	[RhB] = 5 mg/L; 1000 mg/L; 30 min	95.2	95.8	[181]
Black phosphorus (BP)	300 W Xe arc lamp with a UV filter (420 nm < λ < 780 nm)	[TC] = 50 mg/L; 1000 mg/L; 90 min	~ 25	85	[182]
$NaBiO_3$	Fluorescent lamp (22W)	[4CP] = 24 mg/L; 1000 mg/L; 20 min	0.8	> 92	[183]
$La_2Ti_2O_7$	Xe lamp (300 W)	[RhB] = 10 mg/L; 400 mg/L; 20 min	~ 80	~ 100	[184]
CO/ZFO/BOB	150 W LED lamp	[MG] = 25 mg/L; 150 mg/L; 90 min	42	91	[185]
SnO_2	5 W nine parallel LED lights	[RhB] = 20 mg/L; 1000 mg/L; 20 min	~ 60	~ 98.2	[186]
$BiVO_4$	Xe lamp (300 W) with a 420 nm cut-off filter	[RhB] = 10 mg/L; 1000 mg/L; 15 min	~ 60	~ 95	[187]
Bi_5O_7Br	Xe lamp (500 W) with a 420 nm cut-off filter	500 mg/L; [CBZ] = 10 mg/L; 90 min	~ 25.8	~ 90	[188]
Bi(C_2O_4) OH	150 W Xe lamp	1000 mg/L; [RhB] = 10 mg/L; 30 min	89.5	99.6	[189]
Bi12O17Cl2	300 W Xe arc lamp with 420 nm cut-off filter	[MO] = 10 mg/L; 500 mg/L; 20 min	~ 70	~ 92	[190]
BiOCOOH	Xe lamp with a UV filter	[LEV] = 10 mg/L; 600 mg/L; 40 min	75.1	90.1	[191]
CeO_2	300 W Xe lamp with 420 nm cut-off filter	[RhB] = 20 mg/L; 500 mg/L; 25 min	71.2	97.3	[192]
ZnO	300 W iodine-Wolfram lamps	[MB] = 10 mg/L; 1000 mg/L; 240 min	~ 42	~ 90	[193]
ZnS	350 W Xe lamp	[TC] = 20 mg/mL; 1000 mg/L; 25 min	~ 70	~ 82	[194]
Basic bismuth nitrate (BBN)	500 W Xe lamp emitting simulated sunlight	[RhB] = 10 mg/L; 500 mg/L; 45 min	61.8	91.98	[195]
CoS	44 W LED lamp with a UV filter	[GLP] = 10^{-4} mol/L;	21.9	74.7	[196]

		400 mg/L; 180 min			
$Ag_6Si_2O_7$	CEL-HXUB300 Xe lamp equipped with a UV filter (λ ≥ 400 nm)	[MB] = 20 mg/L; 1000 mg/L; 15 min	~ 25	98	[197]
$ZnWO_4$	300 W Xe lamp equipped with a UV cut-off filter (λ ≥ 400 nm)	[RhB] = 2 × 10^{-5} mol/L;500 mg/L; 16 min	~ 50	~ 100	[198]
$SnIn_4S_8$	266 W Xe lamp with a two glass filters (380 nm < λ < 780 nm)	[RhB] = 15 mg/L; 200 mg/L; 40 min	71.1	99.8	[199]
$BiPO_4$	12 W LED light irradiation	[RhB] = 15 mg/L; 1000 mg/L; 120 min	83.51	95.66	[200]
$MnFe_2O_4$	fluorescent lamp (150 W)	[2,4-D] = 20 mg/L; 1000 mg/L; 80 min	57.3	96.5	[201]
C60	Xe lamp (500 W) with a light filter (λ > 420 nm)	[RhB] = 10 mg/L; 1000 mg/L; 10 min	59	91	[202]
NiS	266 W Xe lamp with with a two glass filters (380 nm < λ < 780 nm)	[RhB] = 15 mg/L; 200 mg/L; 50 min	84	99.5	[203]
$SnWO_4$	sunlight radiation (Natural)	[RhB] = 20 mg/L; 1250 mg/L; 60 min	65.9	97.85	[204]
Zn_2GeO_4	Xe lamp equipped with a cut-off filter (λ > 420 nm)	[RhB] = 12 mg/L; 1000 mg/L; 40 min	~ 60	93	[205]
BiOI	500 W Xe lamp passed through annular quartz tube equipped with a cut-off filter (λ > 420 nm)	[MO] = 10 mg/L; 2000 mg/L; 300 min	~ 30	63.1	[206]

*CIP=Ciprofloxacin; CBZ = Carbamazepine; DC = Doxycycline; LEV = Levofloxacin; GLP = Glyphosate; 2,4-D=2,4-dichlorophenoxyacetic acid; RhB = Rhodamine B; TC = Tetracycline; MG = Malachite Green; MO=Methyl Orange; BPA = Bisphenol A; 4CP = 4-chlorophenol; CR = Congo Red; MB = Methylene Blue and W = Watts.

It was concluded that the coupling BiOBr with optimal amount of (CQDs) has the ability for enhancing the photo-catalytic degradation efficiency due to improved optical absorption [155].

7. THE OPERATIONAL PARAMETERS THAT EFFECT ON PHOTO-CATALYTIC DEGRADATION PROCESS

There are several operational conditions that influence on photo-catalytic degradation process are discussed below.

7.1 Initial pH of solution

Initial pH of solution is an important parameter that influences the photo-catalytic degradation efficiency process. Altering the initial solution pH can be Altering by changes in the properties of photo-catalyst's surface charge and the organic pollutant. Many methods have been used for estimating the point of zero charge like potentiometric titration method [136], modified batch equilibrium method [207], salt addition method [165], etc. BiOBr surface is negatively charged at pH above 5.30 and positively charged at pH below 5.30 because the zero charge point of BiOBr was recorded as 5.30 [208].

Also, Wang et al. [209] used BiOBr catalyst for degrading of sulfurhodamine MO, it was found decreasing in the degradation efficiency as pH value increases from 2.0 to 9.0 because low adsorption of sulfurhodamine MO onto the surface of BiOBr due to electrostatic attraction between BiOBr and sulfurhodamine MO. Similarity, by using BiOBr as photo-catalyst for degradation of RhB, it was found that as different values of pH, the performance degradation process was low due to low RhB adsorption onto the surface of BiOBr [210].

Moreover, $BiOBr/ZnFe_2O_4/CuO$ composite has been used for degradation of malachite green (MG) at various pH values (pH=3, 5, 7, 9, and 11), it was noticed that the best (MG) destruction was obtained at pH=7 [103], as shown in Figure 11.

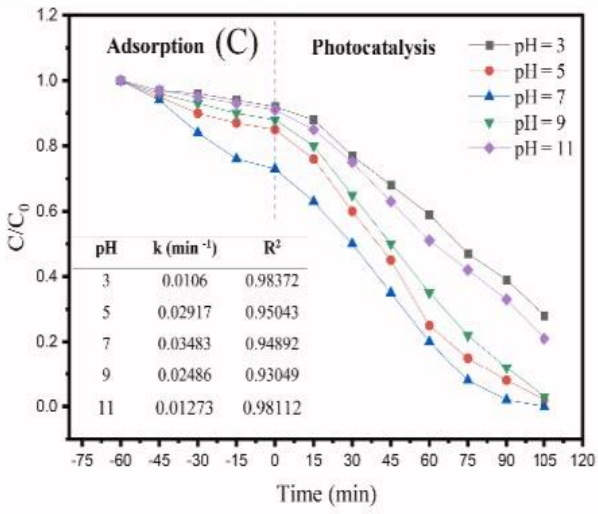

Figure 11. Effect of pH value on MG photo-oxidation over $BiOBr/ZnFe_2O_4/CuO$ [103]

7.2 Catalyst dosage

The BiOBr photo-degradation efficiency is also affected by the dosage of BiOBr catalyst used for degrading of wastewater pollutants, which is lead to increase in the photo-catalytic reactions active surface and increase the photo-generated charge carriers [210-212].

Gondal et al. [213] used BiOBr (600-1500 mg/L) for degrading 7 mg/L of RhB dye and studied the effect of this dosage on the photo-catalytic degradation, with keeping other experimental parameters constant. For 90 min and using 1200 mg/L of BiOBr dosage, it was noticed that 94.6% degradation efficiency was obtained. Then, the degradation efficiency started to reduce. Similarly, it was used BiOBr (250-1500 mg/L) for degrading 10 mg/L of RhB dye and studied the effect of this dosage on the photo-catalytic degradation, it was reported that the optimum BiOBr dosage was 1000 mg/L at the degradation rate of 0.106 per min [210].

7.3 Inorganic ions

Wastewater often contains another pollutant which is inorganic ions [214]. Many authors have reported the effect of these ions on the degradation efficiency. For example, studying the effect of SO_4^{-2}, Cl^-, CO_3^{-2}, PO_4^{-3} and NO_3^- ions on the tetracycline photo-degradation rate using BiOBr. Due to their radical scavenging properties, Cl^- and CO_3^{-2} ions decreased the photo-catalytic activity, while NO_3^-, SO_4^{-2} and PO_4^{-3} did not show any significant inhibition, due to competition among tetracycline and inorganic ions for the BiOBr active sites [215, 216]. Similarly, the effect of SO_4^{-2}, Ca^{+2}, NH_4^+, Cl^-, PO_4^{-3}, CO_3^{-2} and NO_3^-ions on the degradation of ibuprofen was studied. It was found that Cl^-, NH_4^+, Ca^{+2}, SO_4^{-2}, NO_3^- and CO_3^{-2} ions have not significant inhibition effect. While in the presence of PO_4^{-3} ions, the photo-degradation rate was decreased significantly [217, 218].

8. CONCLUSIONS AND RECOMMENDATIONS

In this study, several information associated with BiOBr have been reviewed such as its synthesis, properties, photo-catalytic degradation activity and strategies for improving photo-catalytic efficiency of the BiOBr. Also, it was summarized various operational parameters that effect on BiOBr photo-catalytic degradation rate like initial pH of solution, catalyst dosage and inorganic ions.

Many methods that are used for synthesizing BiOBr, but the most employed methods are solvothermal and hydrothermal methods. By using such methods, various forms of BiOBr photo-catalysis have been synthesized with various features of dimension, pore volume, pore size and morphology. However, the large-scale fabrication of BiOBr must be encouraged with more attractive features.

There are many operational parameters that effect on BiOBr photo-catalytic degradation, including pH of the solution, BiOBr dosage and inorganic ions.

The useful strategies for improving the photo-catalytic performance of BiOBr include formation of composite materials and elemental doping. Even though, the formation of composite materials and elemental doping using facile processes are recommended. Lastly, BiOBr was frequently used for the photo-degradation of pollutants, mostly dyes. So, an important recommendation would be to consider the application of BiOBr in real wastewater treatment. As well as, should be further investigated other potential applications of BiOBr, considering the interesting features of BiOBr.

It should be focusing on developing a recyclable heterojunction with special properties under a UV light which has the ability to degrade non-biodegradable hazardous dye.

REFERENCES

[1] Han, L., Li, B., Wen, H., Guo, Y., Lin, Z. (2021). Photocatalytic degradation of mixed pollutants in aqueous wastewater using mesoporous 2D/2D TiO2 (B)-BiOBr heterojunction. Journal of Materials Science & Technology, 70: 176-184. https://doi.org/10.1016/j.jmst.2020.08.036

[2] Lu, D., Fang, P., Liu, X., Zhai, S., Li, C., Zhao, X., Xiong, R. (2015). A facile one-pot synthesis of TiO_2-based nanosheets loaded with MnxOy nanoparticles with enhanced visible light–driven photocatalytic performance for removal of Cr (VI) or RhB. Applied Catalysis B: Environmental, 179: 558-573. https://doi.org/10.1016/j.apcatb.2015.05.059

[3] Kanakaraju, D., Glass, B.D., Oelgemöller, M. (2014). Titanium dioxide photocatalysis for pharmaceutical wastewater treatment. Environmental Chemistry Letters, 12: 27-47. https://doi.org/10.1007/s10311-013-0428-0

[4] Abdullah, N., Yusof, N., Lau, W.J., Jaafar, J., Ismail, A.F. (2019). Recent trends of heavy metal removal from water/wastewater by membrane technologies. Journal of Industrial and Engineering Chemistry, 76: 17-38. https://doi.org/10.1016/j.jiec.2019.03.029

[5] Singh, A., Pal, D.B., Mohammad, A., Alhazmi, A., Haque, S., Yoon, T., Gupta, V.K. (2022). Biological remediation technologies for dyes and heavy metals in wastewater treatment: New insight. Bioresource Technology, 343: 126154. https://doi.org/10.1016/j.biortech.2021.126154

[6] Martínez-Huitle, C.A., Panizza, M. (2018). Electrochemical oxidation of organic pollutants for wastewater treatment. Current Opinion in Electrochemistry, 11: 62-71. https://doi.org/10.1016/j.coelec.2018.07.010

[7] Wang, W., Li, G., Xia, D., An, T., Zhao, H., Wong, P.K. (2017). Photocatalytic nanomaterials for solar-driven bacterial inactivation: Recent progress and challenges. Environmental Science: Nano, 4(4): 782-799. https://doi.org/10.1039/C7EN00063D

[8] United Nations. (2018). UN World Water Development Report. https://www.unwater.org/publications/un-world-water-development-report.

[9] Mousset, E., Doudrick, K. (2020). A review of electrochemical reduction processes to treat oxidized contaminants in water. Current Opinion in Electrochemistry, 22: 221-227. https://doi.org/10.1016/j.coelec.2020.07.008

[10] Janjhi, F.A., Ihsanullah, I., Bilal, M., Castro-Muñoz, R., Boczkaj, G., Gallucci, F. (2023). MXene-based materials for removal of antibiotics and heavy metals from wastewater–A review. Water Resources and Industry, 29: 100202. https://doi.org/10.1016/j.wri.2023.100202

[11] Ahmed, S.N., Haider, W. (2018). Heterogeneous photocatalysis and its potential applications in water and wastewater treatment: A review. Nanotechnology, 29(34): 342001. https://doi.org/10.1088/1361-6528/aac6ea

[12] Suárez, S., Carballa, M., Omil, F., Lema, J.M. (2008). How are pharmaceutical and personal care products (PPCPs) removed from urban wastewaters? Reviews in Environmental Science and Bio/Technology, 7: 125-138. https://doi.org/10.1007/s11157-008-9130-2

[13] Fedorov, K., Rayaroth, M.P., Shah, N.S., Boczkaj, G. (2023). Activated sodium percarbonate-ozone (SPC/O3) hybrid hydrodynamic cavitation system for advanced oxidation processes (AOPs) of 1, 4-dioxane in water. Chemical Engineering Journal, 456: 141027. https://doi.org/10.1016/j.cej.2022.141027

[14] Zhang, Y., Geißen, S.U., Gal, C. (2008). Carbamazepine and diclofenac: Removal in wastewater treatment plants and occurrence in water bodies. Chemosphere, 73(8): 1151-1161. https://doi.org/10.1016/j.chemosphere.2008.07.086

[15] Zazouli, M.A., Kalankesh, L.R. (2017). Removal of

precursors and disinfection by-products (DBPs) by membrane filtration from water; a review. Journal of Environmental Health Science and Engineering, 15: 1-10. https://doi.org/10.1186/s40201-017-0285-z

[16] Azimi, A., Azari, A., Rezakazemi, M., Ansarpour, M. (2017). Removal of heavy metals from industrial wastewaters: a review. ChemBioEng Reviews, 4(1): 37-59. https://doi.org/10.1002/cben.201600010

[17] Zularisam, A.W., Ismail, A.F., Salim, R. (2006). Behaviours of natural organic matter in membrane filtration for surface water treatment—A review. Desalination, 194(1-3): 211-231. https://doi.org/10.1016/j.desal.2005.10.030

[18] Yu, C., Zhou, W., Yu, J., Cao, F., Li, X. (2012). Thermal stability, microstructure and photocatalytic activity of the bismuth oxybromide photocatalyst. Chinese Journal of Chemistry, 30(3): 721-726. https://doi.org/10.1002/cjoc.201280018

[19] Fernandes, A., Makoś, P., Wang, Z., Boczkaj, G. (2020). Synergistic effect of TiO_2 photocatalytic advanced oxidation processes in the treatment of refinery effluents. Chemical Engineering Journal, 391: 123488. https://doi.org/10.1016/j.cej.2019.123488

[20] Arar, Ö., Yüksel, Ü., Kabay, N., Yüksel, M. (2014). Various applications of electrodeionization (EDI) method for water treatment—A short review. Desalination, 342: 16-22. https://doi.org/10.1016/j.desal.2014.01.028

[21] Li, Z., Meng, X., Zhang, Z. (2019). Fewer-layer BN nanosheets-deposited on Bi2MoO6 microspheres with enhanced visible light-driven photocatalytic activity. Applied Surface Science, 483: 572-580. https://doi.org/10.1016/j.apsusc.2019.03.245

[22] Abid, S., Mustafa, G., Rizwan, M., Iqbal, D.N., Kanwal, S., Ahmad, A., Rasheed, T. (2024). Synthesis of metal oxide nanoparticles using Punica granatum extract for the removal of cationic and anionic dyes from wastewater. Arabian Journal for Science and Engineering, 49(1): 515-530. https://doi.org/10.1007/s13369-023-08166-0

[23] Salimi, F., Emami, S.S., Karami, C. (2018). Removal of methylene blue from water solution by modified nano-boehmite with Bismuth. Inorganic and Nano-Metal Chemistry, 48(1): 31-40. https://doi.org/10.1080/24701556.2017.1357628

[24] Peterson, K.E., Smith, R.C., Mohan, R.S. (2003). Bismuth compounds in organic synthesis. Synthesis of resorcinarenes using bismuth triflate. Tetrahedron Letters, 44(42): 7723-7725. https://doi.org/10.1016/j.tetlet.2003.08.093

[25] Sax, N.I., Bruce, R.D., Durham, W.F. (1975). Dangerous Properties of Industrial Materials, 21. New York: Van Nostrand Reinhold.

[26] Bothwell, J.M., Krabbe, S.W., Mohan, R.S. (2011). Applications of bismuth (III) compounds in organic synthesis. Chemical Society Reviews, 40(9): 4649-4707. https://doi.org/10.1016/S0040-4020(02)01000-1

[27] Jovanovski, V., Hočevar, S.B., Ogorevc, B. (2017). Bismuth electrodes in contemporary electroanalysis. Current Opinion in Electrochemistry, 3(1): 114-122. https://doi.org/10.1016/j.coelec.2017.07.008

[28] Hernandez-Delgadillo, R., García-Cuéllar, C.M., Sánchez-Pérez, Y., Pineda-Aguilar, N., Martínez-Martínez, M.A., Rangel-Padilla, E.E., Cabral-Romero, C. (2018). In vitro evaluation of the antitumor effect of bismuth lipophilic nanoparticles (BisBAL NPs) on breast cancer cells. International Journal of Nanomedicine, 13: 6089-6097. https://doi.org/10.2147/IJN.S179095

[29] Liang, Y., Manioudakis, J., Macairan, J.R., Askari, M.S., Forgione, P., Naccache, R. (2019). Facile aqueous-phase synthesis of an ultrasmall bismuth nanocatalyst for the reduction of 4-nitrophenol. ACS Omega, 4(12): 14955-14961. https://doi.org/10.1021/acsomega.9b01736

[30] Saunders, F. (2010). The disappearing spoon: And other true tales of madness, love, and the history of the world from the periodic table of the elements. American Scientist, 98(5): 438-439.

[31] Maile, F.J., Pfaff, G., Reynders, P. (2005). Effect pigments—past, present and future. Progress in Organic Coatings, 54(3): 150-163. https://doi.org/10.1016/j.porgcoat.2005.07.003

[32] Patil, V.J., Bhoge, Y.E., Patil, U.D., Deshpande, T.D., Kulkarni, R.D. (2016). Room temperature solution spray synthesis of Bismuth Vanadate nanopigment and its utilization in formulation of industrial OEM coatings. Vacuum, 127: 17-21. https://doi.org/10.1016/j.vacuum.2016.02.005

[33] Suzuki, H., Komatsu, N., Ogawa, T., Murafuji, T., Ikegami, T., Matano, Y. (2001). Organobismuth Chemistry. Elsevier.

[34] Lyu, M., Yun, J.H., Chen, P., Hao, M., Wang, L. (2017). Addressing toxicity of lead: Progress and applications of low‐toxic metal halide perovskites and their derivatives. Advanced Energy Materials, 7(15): 1602512. https://doi.org/10.1002/aenm.201602512

[35] Cao, J., Xu, B., Luo, B., Lin, H., Chen, S. (2011). Novel BiOI/BiOBr heterojunction photocatalysts with enhanced visible light photocatalytic properties. Catalysis Communications, 13(1): 63-68. https://doi.org/10.1016/j.catcom.2011.06.019

[36] An, H.Z., Du, Y., Wang, T.M., Wang, C., Hao, W.C., Zhang, J.Y. (2008). Photocatalytic properties of BiOX (X = Cl, Br, and I), Rare Metals, 27(3): 243-250. https://doi.org/10.1016/S1001-0521(08)60123-0

[37] Chang, X., Huang, J., Cheng, C., Sui, Q., Sha, W., Ji, G., Yu, G. (2010). BiOX (X= Cl, Br, I) photocatalysts prepared using NaBiO3 as the Bi source: Characterization and catalytic performance. Catalysis Communications, 11(5): 460-464. https://doi.org/10.1016/j.catcom.2009.11.023

[38] Imam, S.S., Adnan, R., Kaus, N.H.M. (2021). The photocatalytic potential of BiOBr for wastewater treatment: A mini-review. Journal of Environmental Chemical Engineering, 9(4): 105404. https://doi.org/10.1016/j.jece.2021.105404

[39] Wu, D., Yue, S., Wang, W., An, T., Li, G., Yip, H. Y., Wong, P.K. (2016). Boron doped BiOBr nanosheets with enhanced photocatalytic inactivation of Escherichia coli. Applied Catalysis B: Environmental, 192: 35-45. https://doi.org/10.1016/j.apcatb.2016.03.046

[40] Yang, Z., Li, J., Cheng, F., Chen, Z., Dong, X. (2015). BiOBr/protonated graphitic C3N4 heterojunctions: intimate interfaces by electrostatic interaction and enhanced photocatalytic activity. Journal of Alloys and Compounds, 634: 215-222. https://doi.org/10.1016/j.jallcom.2015.02.103

[41] Imam, S.S., Adnan, R., Mohd Kaus, N.H., Hussin, M.H. (2019). Room-temperature synthesis of Bi/BiOBr

composites for the catalytic degradation of ciprofloxacin using indoor fluorescent light illumination. Journal of Materials Science: Materials in Electronics, 30: 6263-6276. https://doi.org/10.1007/s10854-019-00930-z

[42] Guo, J., Liao, X., Lee, M.H., Hyett, G., Huang, C.C., Hewak, D.W., Jiang, Z. (2019). Experimental and DFT insights of the Zn-doping effects on the visible-light photocatalytic water splitting and dye decomposition over Zn-doped BiOBr photocatalysts. Applied Catalysis B: Environmental, 243: 502-512. https://doi.org/10.1016/j.apcatb.2018.09.089

[43] Li, H., Liu, J., Hu, T., Du, N., Song, S., Hou, W. (2016). Synthesis of belt-like BiOBr hierarchical nanostructure with high photocatalytic performance. Materials Research Bulletin, 77: 171-177. https://doi.org/10.1016/j.materresbull.2016.01.039

[44] An, W., Cui, W., Liang, Y., Hu, J., Liu, L. (2015). Surface decoration of BiPO4 with BiOBr nanoflakes to build heterostructure photocatalysts with enhanced photocatalytic activity. Applied Surface Science, 351: 1131-1139. https://doi.org/10.1016/j.apsusc.2015.06.098

[45] Chen, Z., Zeng, J., Di, J., Zhao, D., Ji, M., Xia, J., Li, H. (2017). Facile microwave-assisted ionic liquid synthesis of sphere-like BiOBr hollow and porous nanostructures with enhanced photocatalytic performance. Green Energy & Environment, 2(2): 124-133. https://doi.org/10.1016/j.gee.2017.01.005

[46] Sin, J.C., Lim, C.A., Lam, S.M., Mohamed, A.R. (2017). Surfactant-free hydrothermal synthesis of flower-like BiOBr hierarchical structure and its visible light-driven catalytic activity towards the degradation of sunset yellow. Journal of Materials Science: Materials in Electronics, 28: 13236-13246. https://doi.org/10.1007/s10854-017-7159-0

[47] Zhang, D., Wen, M., Jiang, B., Li, G., Jimmy, C.Y. (2012). Ionothermal synthesis of hierarchical BiOBr microspheres for water treatment. Journal of Hazardous Materials, 211-212: 104-111. https://doi.org/10.1016/j.jhazmat.2011.10.064

[48] Kong, L., Jiang, Z., Lai, H.H., Nicholls, R.J., Xiao, T., Jones, M.O., Edwards, P.P. (2012). Unusual reactivity of visible-light-responsive AgBr–BiOBr heterojunction photocatalysts. Journal of Catalysis, 293: 116-125. https://doi.org/10.1016/j.jcat.2012.06.011

[49] Wang, H.T., Shi, M.S., Yang, H.F., Chang, N., Zhang, H., Liu, Y.P., Chu, D.Q. (2018). Template-free synthesis of nanosliced BiOBr hollow microspheres with high surface area and efficient photocatalytic activity. Materials Letters, 222: 164-167. https://doi.org/10.1016/j.matlet.2018.03.179

[50] Ai, Z., Ho, W., Lee, S. (2011). Efficient visible light photocatalytic removal of NO with BiOBr-graphene nanocomposites. The Journal of Physical Chemistry C, 115(51): 25330-25337. https://doi.org/10.1021/jp206808g

[51] Yuan, M., Tian, F., Li, G., Zhao, H., Liu, Y., Chen, R. (2017). Fe (III)-modified BiOBr hierarchitectures for improved photocatalytic benzyl alcohol oxidation and organic pollutants degradation. Industrial & Engineering Chemistry Research, 56(20): 5935-5943. https://doi.org/10.1021/acs.iecr.7b00905

[52] Shah, N.S., Khan, J.A., Sayed, M., Khan, Z.U.H., Rizwan, A.D., Muhammad, N., Zaman, G. (2018). Solar light driven degradation of norfloxacin using as-synthesized Bi3+ and Fe2+ co-doped ZnO with the addition of HSO5−: Toxicities and degradation pathways investigation. Chemical Engineering Journal, 351: 841-855. https://doi.org/10.1016/j.cej.2018.06.111

[53] Kijima, N., Matano, K., Saito, M., Oikawa, T., Konishi, T., Yasuda, H., Yoshimura, Y. (2001). Oxidative catalytic cracking of n-butane to lower alkenes over layered BiOCl catalyst. Applied Catalysis A: General, 206(2): 237-244. https://doi.org/10.1016/S0926-860X(00)00598-6

[54] Kusainova, A.M., Lightfoot, P., Zhou, W., Stefanovich, S.Y., Mosunov, A.V., Dolgikh, V.A. (2001). Ferroelectric properties and crystal structure of the layered intergrowth phase Bi3Pb2Nb2O11Cl. Chemistry of Materials, 13(12): 4731-4737. https://doi.org/10.1021/cm011145n

[55] Mishra, S.R., Ahmaruzzaman, M. (2021). Cerium oxide and its nanocomposites: Structure, synthesis, and wastewater treatment applications. Materials Today Communications, 28: 102562. https://doi.org/10.1016/j.mtcomm.2021.102562

[56] Ganose, A.M., Cuff, M., Butler, K.T., Walsh, A., Scanlon, D.O. (2016). Interplay of orbital and relativistic effects in bismuth oxyhalides: BiOF, BiOCl, BiOBr, and BiOI. Chemistry of Materials, 28(7): 1980-1984. https://doi.org/10.1021/acs.chemmater.6b00349

[57] Saber, N.B., Mezni, A., Alrooqi, A., Altalhi, T. (2020). A review of ternary nanostructures based noble metal/semiconductor for environmental and renewable energy applications. Journal of Materials Research and Technology, 9(6): 15233-15262. https://doi.org/10.1016/j.jmrt.2020.10.090

[58] Prasad, C., Tang, H., Bahadur, I. (2019). Graphitic carbon nitride based ternary nanocomposites: From synthesis to their applications in photocatalysis: A recent review. Journal of Molecular Liquids, 281: 634-654. https://doi.org/10.1016/j.molliq.2019.02.068

[59] Arumugam, M., Natarajan, T.S., Saelee, T., Praserthdam, S., Ashokkumar, M., Praserthdam, P. (2021). Recent developments on bismuth oxyhalides (BiOX; X= Cl, Br, I) based ternary nanocomposite photocatalysts for environmental applications. Chemosphere, 282: 131054. https://doi.org/10.1016/j.chemosphere.2021.131054

[60] Zheng, M., Ma, X., Hu, J., Zhang, X., Li, D., Duan, W. (2020). Novel recyclable BiOBr/Fe_3O_4/RGO composites with remarkable visible-light photocatalytic activity. RSC Advances, 10(34): 19961-19973. https://doi.org/10.1039/D0RA01668C

[61] Shih, K.Y., Kuan, Y.L., Wang, E.R. (2021). One-step microwave-assisted synthesis and visible-light photocatalytic activity enhancement of BiOBr/RGO nanocomposites for degradation of methylene blue. Materials, 14(16): 4577. https://doi.org/10.3390/ma14164577

[62] Braslavsky, S.E. (2007). Glossary of terms used in photochemistry, (IUPAC Recommendations 2006). Pure and Applied Chemistry, 79(3): 293-465. https://doi.org/10.1351/pac200779030293

[63] Liu, J., Zheng, Z., Zuo, K., Wu, Y. (2006). Preparation and characterization of Fe 3+-doped nanometer TiO_2 photocatalysts. Journal of Wuhan University of Technology-Materials Science Edition, 21(3): 57-60. https://doi.org/10.1007/BF02840880

[64] Van Gerven, T., Mul, G., Moulijn, J., Stankiewicz, A. (2007). A review of intensification of photocatalytic processes. Chemical Engineering and Processing: Process Intensification, 46(9): 781-789. https://doi.org/10.1016/j.cep.2007.05.012
[65] Tayade, R.J., Natarajan, T.S., Bajaj, H.C. (2009). Photocatalytic degradation of methylene blue dye using ultraviolet light emitting diodes. Industrial & Engineering Chemistry Research, 48(23): 10262-10267. https://doi.org/10.1021/ie9012437
[66] Li, Y., Li, X., Li, J., Yin, J. (2006). Photocatalytic degradation of methyl orange by TiO_2-coated activated carbon and kinetic study. Water Research, 40(6): 1119-1126. https://doi.org/10.1016/j.watres.2005.12.042
[67] Hu, Q., Liu, B., Zhang, Z., Song, M., Zhao, X. (2010). Temperature effect on the photocatalytic degradation of methyl orange under UV-vis light irradiation. Journal of Wuhan University of Technology-Materials Science Edition, 25(2): 210-213. https://doi.org/10.1007/s11595-010-2210-5
[68] Zhang, S., Chen, Z., Li, Y., Wang, Q., Wan, L. (2008). Photocatalytic degradation of methylene blue in a sparged tube reactor with TiO_2 fibers prepared by a properly two-step method. Catalysis Communications, 9(6): 1178-1183. https://doi.org/10.1016/j.catcom.2007.11.009
[69] Skocaj, M., Filipic, M., Petkovic, J., Novak, S. (2011). Titanium dioxide in our everyday life; is it safe? Radiology and Oncology, 45(4): 227-247. https://doi.org/10.2478/v10019-011-0037-0
[70] Kim, G., Park, Y., Moon, G. H., Choi, W. (2016). Photoexcitation in pure and modified semiconductor photocatalysts. In Photocatalysis: Fundamentals and Perspectives, the Royal Society of Chemistry, UK, pp. 110-128. https://doi.org/10.1039/9781782622338-00110
[71] Zhang, X., Qin, J., Xue, Y., Yu, P., Zhang, B., Wang, L., Liu, R. (2014). Effect of aspect ratio and surface defects on the photocatalytic activity of ZnO nanorods. Scientific Reports, 4(1): 4596. https://doi.org/10.1038/srep04596
[72] Herrmann, J.M. (2005). Heterogeneous photocatalysis: state of the art and present applications in honor of Pr. RL Burwell Jr. (1912-2003): Former Head of Ipatieff Laboratories, Northwestern University, Evanston (Ill). Topics in Catalysis, 34: 49-65. https://doi.org/10.1007/s11244-005-3788-2
[73] Chang, J., Waclawik, E.R. (2012). Facet-controlled self-assembly of ZnO nanocrystals by non-hydrolytic aminolysis and their photodegradation activities. CrystEngComm, 14(11): 4041-4048. https://doi.org/10.1039/C2CE25154J
[74] Jiang, Z., Yang, F., Yang, G., Kong, L., Jones, M. O., Xiao, T., Edwards, P.P. (2010). The hydrothermal synthesis of BiOBr flakes for visible-light-responsive photocatalytic degradation of methyl orange. Journal of Photochemistry and Photobiology A: Chemistry, 212(1): 8-13. https://doi.org/10.1016/j.jphotochem.2010.03.004
[75] Liu, Y., Zhang, X., Li, X., Zhou, Z. (2024). Visible light driven S-scheme GQDs/BiOBr heterojunction with enhanced photocatalytic degradation of Rhodamine B and mechanism insight. Journal of Water Process Engineering, 57: 104588. https://doi.org/10.1016/j.jwpe.2023.104588
[76] Wang, Y., Tao, R., Yan, T., Fan, X., Liu, K. (2023). Construction of flexible Biobr/W18o49/Polyacrylonitrile discrete heterojunction nanofibers as a dual-functional photocatalyst for simultaneous hydrogen evolution and organic pollutant degradation. https://doi.org/10.2139/ssrn.4587294
[77] Nyankson, E., Agyei-Tuffour, B., Asare, J., Annan, E., Rwenyagila, E.R., Konadu, D.S., Dodoo-Arhin, D. (2013). Nanostructured TiO_2 and their energy applications-a review. ARPN Journal of Engineering and Applied Sciences, 8(10): 871-886.
[78] Yang, X., Wang, Y., Xu, L., Yu, X., Guo, Y. (2008). Silver and indium oxide codoped TiO_2 nanocomposites with enhanced photocatalytic activity. The Journal of Physical Chemistry C, 112(30): 11481-11489. https://doi.org/10.1021/jp803559g
[79] Shehu Imam, S., Adnan, R., Mohd Kaus, N.H. (2018). Photocatalytic degradation of ciprofloxacin in aqueous media: A short review. Toxicological & Environmental Chemistry, 100(5-7): 518-539. https://doi.org/10.1080/02772248.2018.1545128
[80] Pelaez, M., Nolan, N.T., Pillai, S.C., Seery, M.K., Falaras, P., Kontos, A.G., Dionysiou, D.D. (2012). A review on the visible light active titanium dioxide photocatalysts for environmental applications. Applied Catalysis B: Environmental, 125: 331-349. https://doi.org/10.1016/j.apcatb.2012.05.036
[81] Chong, M.N., Jin, B., Chow, C.W., Saint, C. (2010). Recent developments in photocatalytic water treatment technology: A review. Water Research, 44(10): 2997-3027. https://doi.org/10.1016/j.watres.2010.02.039
[82] Intaphong, P., Phuruangrat, A., Karthik, K., Dumrongrojthanath, P., Thongtem, T., Thongtem, S. (2020). Effect of pH on phase, morphology and photocatalytic properties of BiOBr synthesized by hydrothermal method. Journal of Inorganic and Organometallic Polymers and Materials, 30: 714-721. https://doi.org/10.1007/s10904-019-01259-0
[83] Fu, S.M., Li, G.S., Xing, W.E.N., Fan, C.M., Liu, J.X., Zhang, X.C., Rui, L.I. (2020). Effect of calcination temperature on microstructure and photocatalytic activity of BiOX (X= Cl, Br). Transactions of Nonferrous Metals Society of China, 30(3): 765-773. https://doi.org/10.1016/s1003-6326(20)65252-9
[84] Lyu, J., Li, Z., Ge, M. (2018). Novel Bi/BiOBr/AgBr composite microspheres: Ion exchange synthesis and photocatalytic performance. Solid State Sciences, 80: 101-109. https://doi.org/10.1016/j.solidstatesciences.2018.04.004
[85] Mi, Y., Li, H., Zhang, Y., Hou, W. (2019). Synthesis of belt-like bismuth-rich bismuth oxybromide hierarchical nanostructures with high photocatalytic activities. Journal of Colloid and Interface Science, 534: 301-311. https://doi.org/10.1016/j.jcis.2018.09.038
[86] Li, C., Wang, B., Zhang, F., Song, N., Liu, G., Wang, C., Zhong, S. (2020). Performance of Ag/BiOBr/GO composite photocatalyst for visible-light-driven dye pollutants degradation. Journal of Materials Research and Technology, 9(1): 610-621. https://doi.org/10.1016/j.jmrt.2019.11.001
[87] Qu, J., Du, Y., Feng, Y., Wang, J., He, B., Du, M., Jiang, N. (2020). Visible-light-responsive K-doped g-C3N4/BiOBr hybrid photocatalyst with highly efficient degradation of Rhodamine B and tetracycline. Materials Science in Semiconductor Processing, 112: 105023. https://doi.org/10.1016/j.mssp.2020.105023

[88] Guo, Y., Zhang, J., Zhou, D., Dong, S. (2018). Fabrication of Ag/CDots/BiOBr ternary photocatalyst with enhanced visible-light driven photocatalytic activity for 4-chlorophenol degradation. Journal of Molecular Liquids, 262: 194-203. https://doi.org/10.1016/j.molliq.2018.04.091

[89] Jiang, Y.R., Chou, S.Y., Chang, J.L., Huang, S.T., Lin, H.P., Chen, C.C. (2015). Hydrothermal synthesis of bismuth oxybromide–bismuth oxyiodide composites with high visible light photocatalytic performance for the degradation of CV and phenol. RSC Advances, 5(39): 30851-30860. https://doi.org/10.1039/C5RA01702E

[90] Gao, M., Zhang, D., Pu, X., Li, H., Lv, D., Zhang, B., Shao, X. (2015). Facile hydrothermal synthesis of Bi/BiOBr composites with enhanced visible-light photocatalytic activities for the degradation of rhodamine B. Separation and Purification Technology, 154: 211-216. https://doi.org/10.1016/j.seppur.2015.09.063

[91] Wang, Q.S., Teng, Y., Xia, J., Zhao, L., Ruan, M.M. (2015). Improved photocatalytic performance of self-assembled Bi/BiOBr square microflowers with square nanopetals. RSC Advances, 5(98): 80853-80858. https://doi.org/10.1039/C5RA16571G

[92] Cheng, H., Huang, B., Wang, P., Wang, Z., Lou, Z., Wang, J., Dai, Y. (2011). In situ ion exchange synthesis of the novel Ag/AgBr/BiOBr hybrid with highly efficient decontamination of pollutants. Chemical Communications, 47(25): 7054-7056. https://doi.org/10.1039/C1CC11525A

[93] Liu, Z., Wu, B., Xiang, D., Zhu, Y. (2012). Effect of solvents on morphology and photocatalytic activity of BiOBr synthesized by solvothermal method. Materials Research Bulletin, 47(11): 3753-3757. https://doi.org/10.1016/j.materresbull.2012.06.026

[94] Li, J., Yang, F., Zhou, Q., Wu, L., Li, W., Ren, R., Lv, Y. (2019). Visible-light photocatalytic performance, recovery and degradation mechanism of ternary magnetic Fe_3O_4/BiOBr/BiOI composite. RSC Advances, 9(41): 23545-23553. https://doi.org/10.1039/C9RA04412D

[95] Li, W., Tian, Y., Li, P., Zhang, B., Zhang, H., Geng, W., Zhang, Q. (2015). Synthesis of rattle-type magnetic mesoporous Fe_3O_4@/mSiO_2@BiOBr hierarchical photocatalyst and investigation of its photoactivity in the degradation of methylene blue. RSC Advances, 5(59): 48050-48059.

[96] Senasu, T., Nijpanich, S., Juabrum, S., Chanlek, N., Nanan, S. (2021). CdS/BiOBr heterojunction photocatalyst with high performance for solar-light-driven degradation of ciprofloxacin and norfloxacin antibiotics. Applied Surface Science, 567: 150850. https://doi.org/10.1016/j.apsusc.2021.150850

[97] Zhang, J., Xia, J., Yin, S., Li, H., Xu, H., He, M., Zhang, Q. (2013). Improvement of visible light photocatalytic activity over flower-like BiOCl/BiOBr microspheres synthesized by reactable ionic liquids. Colloids and Surfaces A: Physicochemical and Engineering Aspects, 420: 89-95. https://doi.org/10.1016/j.colsurfa.2012.11.054

[98] Zhang, R., Han, Q., Li, Y., Zhang, T., Liu, Y., Zeng, K., Zhao, C. (2020). Solvothermal synthesis of a peony flower-like dual Z-scheme PANI/BiOBr/$ZnFe_2O_4$ photocatalyst with excellent photocatalytic redox activity for organic pollutant under visible-light. Separation and Purification Technology, 234: 116098. https://doi.org/10.1016/j.seppur.2019.116098

[99] Lu, L., Zhou, M.Y., Yin, L., Zhou, G.W., Jiang, T., Wan, X.K., Shi, H.X. (2016). Tuning the physicochemical property of BiOBr via pH adjustment: Towards an efficient photocatalyst for degradation of bisphenol A. Journal of Molecular Catalysis A: Chemical, 423: 379-385. https://doi.org/10.1016/j.molcata.2016.07.017

[100] Gao, M., Zhang, D., Pu, X., Ma, H., Su, C., Gao, X., Dou, J. (2016). Surface decoration of BiOBr with $BiPO_4$ nanoparticles to build heterostructure photocatalysts with enhanced visible-light photocatalytic activity. Separation and Purification Technology, 170: 183-189. https://doi.org/10.1016/j.seppur.2016.06.045

[101] Cheng, L., Hu, X., Hao, L. (2018). Ultrasonic-assisted in-situ fabrication of BiOBr modified $Bi_2O_2CO_3$ microstructure with enhanced photocatalytic performance. Ultrasonics Sonochemistry, 44: 137-145. https://doi.org/10.1016/j.ultsonch.2018.02.023

[102] Zhao, Y., Huang, X., Tan, X., Yu, T., Li, X., Yang, L., Wang, S. (2016). Fabrication of BiOBr nanosheets@ TiO_2 nanobelts p–n junction photocatalysts for enhanced visible-light activity. Applied Surface Science, 365: 209-217. https://doi.org/10.1016/j.apsusc.2015.12.249

[103] Sabit, D.A., Ebrahim, S.E. (2023). Fabrication of magnetic BiOBr/$ZnFe_2O_4$/CuO heterojunction for improving the photocatalytic destruction of malachite green dye under LED irradiation: Dual S-scheme mechanism. Materials Science in Semiconductor Processing, 163: 107559. https://doi.org/10.1016/j.mssp.2023.107559

[104] Lee, S.Y., Park, S.J. (2013). TiO_2 photocatalyst for water treatment applications. Journal of industrial and engineering chemistry, 19(6): 1761-1769. https://doi.org/10.1016/j.jiec.2013.07.012

[105] Ahmed, S., Ollis, D.F. (1984). Solar photoassisted catalytic decomposition of the chlorinated hydrocarbons trichloroethylene and trichloromethane. Solar Energy, 32: 597-601. https://doi.org/10.1016/0038-092X(84)90135-X

[106] Hoffmann, M.R., Martin, S.T., Choi, W., Bahnemann, D.W. (1995). Environmental applications of semiconductor photocatalysis. Chemical Reviews, 95(1): 69-96. https://doi.org/10.1021/cr00033a004

[107] Schiavello, M., Sclafani, A. (1989). Thermodynamic and kinetic aspects in photocatalysis. Photocatalysis: Fundamentals and Applications. John Wiley & Sons, 159-173.

[108] Han, A., Zhang, H., Lu, D., Sun, J., Chuah, G.K., Jaenicke, S. (2018). Efficient photodegradation of chlorophenols by BiOBr/$NaBiO_3$ heterojunctioned composites under visible light. Journal of hazardous materials, 341: 83-92. https://doi.org/10.1016/j.jhazmat.2017.07.031

[109] Xie, X., Li, S., Qi, K., Wang, Z. (2021). Photoinduced synthesis of green photocatalyst Fe_3O_4/BiOBr/CQDs derived from corncob biomass for carbamazepine degradation: the role of selectively more CQDs decoration and Z-scheme structure. Chemical Engineering Journal, 420: 129705. https://doi.org/10.1016/j.cej.2021.129705

[110] Rashid, J., Abbas, A., Chang, L.C., Iqbal, A., Haq, I.U., Rehman, A., Awan, S.U., Arshad, M., Barakat, M.A. (2019). Butterfly cluster like lamellar BiOBr/TiO_2

nanocomposite for enhanced sunlight photocatalytic mineralization of aqueous ciprofloxacin. Science of the Total Environment, 665: 668-677. https://doi.org/10.1016/j.scitotenv.2019.02.145

[111] Wei, X.X., Cui, H., Guo, S., Zhao, L., Li, W. (2013). Hybrid BiOBr–TiO_2 nanocomposites with high visible light photocatalytic activity for water treatment. Journal of Hazardous Materials, 263: 650-658. https://doi.org/10.1016/j.jhazmat.2013.10.027

[112] Wei, X.X., Chen, C. M., Guo, S.Q., Guo, F., Li, X.M., Wang, X.X., Cui, H.T., Zhao, L.F. Li, W. (2014). Advanced visible-light-driven photocatalyst BiOBr–TiO_2–graphene composite with graphene as a nano-filler. Journal of Materials Chemistry A, 2(13): 4667-4675. https://doi.org/10.1039/C3TA14349J

[113] Wang, X.J., Yang, W.Y., Li, F.T., Zhao, J., Liu, R.H., Liu, S.J., Li, B. (2015). Construction of amorphous TiO_2/BiOBr heterojunctions via facets coupling for enhanced photocatalytic activity. Journal of Hazardous Materials, 292: 126-136. https://doi.org/10.1016/j.jhazmat.2015.03.030

[114] Yang, X., Chen, Z., Zhao, W., Liu, C., Qian, X., Chang, W., Sun, T., Shen, T., Wei, G. (2021). Construction of porous-hydrangea BiOBr/BiOI nn heterojunction with enhanced photodegradation of tetracycline hydrochloride under visible light. Journal of Alloys and Compounds, 864: 158784. https://doi.org/10.1016/j.jallcom.2021.158784

[115] Wang, Y., Long, Y., Yang, Z., Zhang, D. (2018). A novel ion-exchange strategy for the fabrication of high strong BiOI/BiOBr heterostructure film coated metal wire mesh with tunable visible-light-driven photocatalytic reactivity. Journal of hazardous materials, 351: 11-19. https://doi.org/10.1016/j.jhazmat.2018.02.027

[116] Liu, B., Han, X., Wang, Y., Fan, X., Wang, Z., Zhang, J., Shi, H. (2018). Synthesis of g-C_3N_4/BiOI/BiOBr heterostructures for efficient visible-light-induced photocatalytic and antibacterial activity. Journal of Materials Science: Materials in Electronics, 29: 14300-14310. https://doi.org/10.1007/s10854-018-9564-4

[117] Yuan, D., Huang, L., Li, Y., Xu, Y., Xu, H., Huang, S., Yan, J., He, M.Q. Li, H. (2016). Synthesis and photocatalytic activity of g-C_3N_4/BiOI/BiOBr ternary composites. RSC advances, 6(47): 41204-41213. https://doi.org/10.1039/C6RA05565F

[118] Cao, J., Xu, B., Lin, H., Luo, B., Chen, S. (2012). Chemical etching preparation of BiOI/BiOBr heterostructures with enhanced photocatalytic properties for organic dye removal. Chemical Engineering Journal, 185: 91-99. https://doi.org/10.1016/j.cej.2012.01.035

[119] Zhang, L., Tan, L., Yuan, Z., Xu, B., Chen, W., Tang, Y., Li, L., Wang, J. (2023). Engineering of $Bi_2O_2CO_3$/Ti_3C_2Tx heterojunctions co-embedded with surface and interface oxygen vacancies for boosted photocatalytic degradation of levofloxacin. Chemical Engineering Journal, 452(Part 2): 139327. https://doi.org/10.1016/j.cej.2022.139327

[120] Bayarri, B., Gimenez, J., Curco, D., Esplugas, S. (2005). Photocatalytic degradation of 2, 4-dichlorophenol by TiO_2/UV: kinetics, actinometries and models. Catalysis Today, 101(3-4): 227-236.

[121] Puma, G.L., Yue, P.L. (2002). Effect of radiation wavelength on the rate of photocatalytic oxidation of organic pollutants. Industrial & Engineering Chemistry Research, 41: 5594-5600. https://doi.org/10.1021/ie0203274

[122] Jabbar, Z.H., Ebrahim, S.E. (2021). Highly efficient visible-light-driven photocatalytic degradation of organic pollutants by using magnetically separable supported heterogeneous nanocomposites (SiO_2/Fe_3O_4/Ag_2WO_4). Environmental Nanotechnology, Monitoring & Management, 16: 100554. https://doi.org/10.1016/j.enmm.2021.100554

[123] Xia, J., Yin, S., Li, H., Xu, H., Xu, L., Xu, Y. (2011). Improved visible light photocatalytic activity of sphere-like BiOBr hollow and porous structures synthesized via a reactable ionic liquid. Dalton Transactions, 40: 5249-5258. https://doi.org/10.1039/C0DT01511C

[124] Xue, C., Xia, J., Wang, T., Zhao, S., Yang, G., Yang, B., Dai, Y., Yang, G. (2014). A facile and efficient solvothermal fabrication of three-dimensionally hierarchical BiOBr microspheres with exceptional photocatalytic activity. Materials Letters, 133: 274-277. https://doi.org/10.1016/j.matlet.2014.07.016

[125] Ye, L., Su, Y., Jin, X., Xie, H., Cao, F., Guo, Z. (2014). Which affect the photo reactivity of BiOBr single-crystalline nanosheets with different hydrothermal pH value: Size or facet? Applied Surface Science, 311: 858-863. https://doi.org/10.1016/j.apsusc.2014.05.191

[126] Danish, M., Muneer, M. (2021). Excellent visible-light-driven Ni-ZnS/g-C_3N_4 photocatalyst for enhanced pollutants degradation performance: Insight into the photocatalytic mechanism and adsorption isotherm. Applied Surface Science, 563: 150262. https://doi.org/10.1016/j.apsusc.2021.150262

[127] Shariati, M.R., Samadi-Maybodi, A., Colagar, A.H. (2019). Exploration of charge carrier delocalization in the iron oxide/CdS type-II heterojunction band alignment for enhanced solar-driven photocatalytic and antibacterial applications. Journal of Hazardous Materials, 366: 475-481. https://doi.org/10.1016/j.jhazmat.2018.12.025

[128] Wei, X.X., Cui, H., Guo, S., Zhao, L., Li, W. (2013). Hybrid BiOBr-TiO_2 nanocomposites with high visible light photocatalytic activity for water treatment. Journal of Hazardous Materials, 263: 650-658. https://doi.org/10.1016/j.jhazmat.2013.10.027

[129] Kalyanasundaram, K., Gratzel, M., Peliuetti, E. (1985). Coord. Chem. Rev., 69: 57.

[130] Zhang, Z., Zhang, Y., Wang, J., Xu, J., Long, R. (2021). Doping-induced charge localization suppresses electron-hole recombination in copper zinc tin sulfide: quantum dynamics combined with deep neural networks analysis. The Journal of Physical Chemistry Letters, 12(2): 835-842. https://doi.org/10.1021/acs.jpclett.0c03522

[131] Liu, Z., Wu, B., Zhu, Y., Yin, D., Wang, L. (2012). Fe-ions modified BiOBr mesoporous microspheres with excellent photocatalytic property. Catalysis Letters, 142: 1489-1497. https://doi.org/10.1007/s10562-012-0899-9

[132] Tu, X., Qian, S., Chen, L., Qu, L. (2015). The influence of Sn (II) doping on the photoinduced charge and photocatalytic properties of BiOBr microspheres. Journal of Materials Science, 50: 4312-4323. https://doi.org/10.1007/s10853-015-8983-3

[133] Song, X.C., Zheng, Y.F., Yin, H.Y., Liu, J.N., Ruan,

X.D. (2016). The solvothermal synthesis and enhanced photocatalytic activity of Zn^{2+} doped BiOBr hierarchical nanostructures. New Journal of Chemistry, 40: 130-135. https://doi.org/10.1039/C5NJ01282A

[134] Devi, L.G., Rajashekhar, K.E. (2011). A kinetic model based on non-linear regression analysis is proposed for the degradation of phenol under UV/solar light using nitrogen doped TiO_2. Journal of Molecular Catalysis A: Chemical, 334(1-2): 65-76. https://doi.org/10.1016/j.molcata.2010.10.025

[135] Devi, L.G., Krishnamurthy, G. (2011). TiO_2-and $BaTiO_3$-assisted photocatalytic degradation of selected chloroorganic compounds in aqueous medium: correlation of reactivity/orientation effects of substituent groups of the pollutant molecule on the degradation rate. The Journal of Physical Chemistry A, 115(4): 460-469. https://doi.org/10.1021/jp103301z

[136] Meng, X., Li, Z., Chen, J., Xie, H., Zhang, Z. (2018). Enhanced visible light-induced photocatalytic activity of surface-modified BiOBr with Pd nanoparticles. Applied Surface Science, 433: 76-87. https://doi.org/10.1016/j.apsusc.2017.09.103

[137] Li, X., Mao, X., Zhang, X., Wang, Y., Wang, Y., Zhang, H., Hao, X., Fan, C. (2015). Citric acid-assisted synthesis of nano-Ag/BiOBr with enhanced photocatalytic activity. Science China Chemistry, 58: 457-466. https://doi.org/10.1007/s11426-014-5152-5

[138] Dou, Y., Yuan, D., Yu, L., Zhang, W., Zhang, L., Fan, K., Al-Mamun, M., Liu, P., He, C.T., Zhao, H. (2022). Interpolation between W dopant and Co vacancy in CoOOH for enhanced oxygen evolution catalysis. Advanced Materials, 34(2): 2104667. https://doi.org/10.1002/adma.202104667

[139] Liu, Z., Liu, J., Wang, H., Cao, G., Niu, J. (2016). Boron-doped bismuth oxybromide microspheres with enhanced surface hydroxyl groups: Synthesis, characterization and dramatic photocatalytic activity. Journal of Colloid and Interface Science, 463: 324-331. https://doi.org/10.1016/j.jcis.2015.10.028

[140] Huang, M., Li, J., Su, W., Huang, X., Li, B., Fan, M., Dong, L.H., He, H. (2020). Oriented construction of S-doped, exposed {001} facet BiOBr nanosheets with abundant oxygen vacancies and promoted visible-light-driven photocatalytic performance. CrystEngComm, 22(44): 7684-7692. https://doi.org/10.1039/D0CE01187H

[141] Wang, R., Jiang, G., Wang, X., Hu, R., Xi, X., Bao, S., Zhou, Y., Tong, T., Wang, S., Wang, T. (2012). Efficient visible-light-induced photocatalytic activity over the novel Ti-doped BiOBr microspheres. Powder Technology, 228: 258-263. https://doi.org/10.1016/j.powtec.2012.05.028

[142] Lv, X., Yan, D.Y., Lam, F.L.Y., Ng, Y.H., Yin, S., An, A.K. (2020). Solvothermal synthesis of copper-doped BiOBr microflowers with enhanced adsorption and visible-light driven photocatalytic degradation of norfloxacin. Chemical Engineering Journal, 401: 126012. https://doi.org/10.1016/j.cej.2020.126012

[143] Huang, W., Hua, X., Zhao, Y., Li, K., Tang, L., Zhou, M., Cai, Z. (2019). Enhancement of visible-light-driven photocatalytic performance of BiOBr nanosheets by Co^{2+} doping. Journal of Materials Science: Materials in Electronics, 30: 14967-14976. https://doi.org/10.1007/s10854-019-01869-x

[144] Wei, Z., Jiang, G., Shen, L., Li, X., Wang, X., Chen, W. (2013). Preparation of Mn-doped BiOBr microspheres for efficient visible-light-induced photocatalysis. MRS Communications, 3: 145-149. https://doi.org/10.1557/mrc.2013.29

[145] Wei, Z., Dong, X., Zheng, N., Wang, Y., Zhang, X., Ma, H. (2020). Novel visible-light irradiation niobium-doped BiOBr microspheres with enhanced photocatalytic performance. Journal of Materials Science, 55: 16522-16532. ttps://doi.org/10.1007/s10853-020-05265-3

[146] Li, X., Jiang, G., Wei, Z., Wang, X., Chen, W., Shen, L. (2013). One-pot solvothermal preparation of S-doped BiOBr microspheres for efficient visible-light induced photocatalysis. MRS Communications, 3(3): 219-224. https://doi.org/10.1557/mrc.2013.34

[147] Bi, C., Cao, J., Lin, H., Wang, Y., Chen, S. (2016). Tunable photocatalytic and photoelectric properties of I-doped BiOBr photocatalyst: Dramatic pH effect. RSC Advances, 6(17): 15525-15534. https://doi.org/10.1016/j.cej.2020.125258

[148] Cao, F., Wang, J., Wang, Y., Zhou, J., Li, S., Qin, G., Fan, W. (2019). An in-situ Bi-decorated BiOBr photocatalyst for synchronously treating multiple antibiotics in water. Nanoscale Advances, 1(3): 1124-1129. https://doi.org/10.1039/C8NA00197A

[149] Imam, S.S., Adnan, R., Kaus, N.H.M. (2018). Influence of yttrium doping on the photocatalytic activity of bismuth oxybromide for ciprofloxacin degradation using indoor fluorescent light illumination. Research on Chemical Intermediates, 44(12): 5357-5376. https://doi.org/10.1007/s11164-018-3427-8

[150] Jabbar, Z.H., Ebrahim, S.E. (2021). Synthesis, characterization, and photocatalytic degradation activity of core/shell magnetic nanocomposites (Fe_3O_4@SiO_2@Ag_2WO_4@Ag_2S) under visible light irradiation. Optical Materials, 122(Part B): 111818. https://doi.org/10.1016/j.optmat.2021.111818

[151] Ling, F., Li, W., Ye, L. (2019). The synergistic effect of non-metal doping or defect engineering and interface coupling on the photocatalytic property of g-C_3N_4: First-principle investigations. Applied Surface Science, 473: 386-392. https://doi.org/10.1016/j.apsusc.2018.12.085

[152] Hosseini, S.M., Safarifard, V. (2024). MoS_2@ MOF composites: Design strategies and photocatalytic applications. Materials Science in Semiconductor Processing, 169: 107892. https://doi.org/10.1016/j.mssp.2023.107892

[153] Qiu, F., Li, W., Wang, F., Li, H., Liu, X., Ren, C. (2017). Preparation of novel PN heterojunction $Bi_2O_2CO_3$/BiOBr photocatalysts with enhanced visible light photocatalytic activity. Colloids and Surfaces A: Physicochemical and Engineering Aspects, 517: 25-32. https://doi.org/10.1016/j.colsurfa.2017.01.008

[154] Su, X., Wu, D. (2018). Facile construction of the phase junction of BiOBr and $Bi_4O_5Br_2$ nanoplates for ciprofloxacin photodegradation. Materials Science in Semiconductor Processing, 80: 123-130. https://doi.org/10.1016/j.mssp.2018.02.034

[155] Xia, J., Di, J., Li, H., Xu, H., Li, H., Guo, S. (2016). Ionic liquid-induced strategy for carbon quantum dots/BiOX (X= Br, Cl) hybrid nanosheets with superior visible light-driven photocatalysis. Applied Catalysis B: Environmental, 181: 260-269. https://doi.org/10.1016/j.apcatb.2015.07.035

[156] Cheng, L., Hu, X., Hao, L. (2018). Ultrasonic-assisted in-situ fabrication of BiOBr modified $Bi_2O_2CO_3$ microstructure with enhanced photocatalytic performance. Ultrasonics Sonochemistry, 44: 137-145. https://doi.org/10.1016/j.ultsonch.2018.02.023

[157] Cui, H., Zhou, Y., Mei, J., Li, Z., Xu, S., Yao, C. (2018). Synthesis of CdS/BiOBr nanosheets composites with efficient visible-light photocatalytic activity. Journal of Physics and Chemistry of Solids, 112: 80-87. https://doi.org/10.1016/j.jpcs.2017.09.011

[158] Li, X., Wang, L., Zhang, L., Zhuo, S. (2017). A facile route to the synthesis of magnetically separable BiOBr/$NiFe_2O_4$ composites with enhanced photocatalytic performance. Applied Surface Science, 419: 586-594. https://doi.org/10.1016/j.apsusc.2017.05.013

[159] Mao, W., Bao, K., Cao, F., Chen, B., Liu, G., Wang, W., Li, B. (2017). Synthesis of a $CoTiO_3$/BiOBr heterojunction composite with enhanced photocatalytic performance. Ceramics International, 43(3): 3363-3368. https://doi.org/10.1016/j.ceramint.2016.11.180

[160] Xing, Y., He, Z., Que, W. (2016). Synthesis and characterization of ZnO nanospheres sensitized BiOBr plates with enhanced photocatalytic performances. Materials Letters, 182: 210-213. https://doi.org/10.1016/j.matlet.2016.06.122

[161] Jiang, R., Zhu, H.Y., Li, J. B., Fu, F.Q., Yao, J., Jiang, S.T., Zeng, G.M. (2016). Fabrication of novel magnetically separable BiOBr/$CoFe_2O_4$ microspheres and its application in the efficient removal of dye from aqueous phase by an environment-friendly and economical approach. Applied Surface Science, 364: 604-612. https://doi.org/10.1016/j.apsusc.2015.12.200

[162] Rashid, J., Abbas, A., Chang, L.C., Iqbal, A., Ul Haq, I., Rehman, A., Awan, S.U., Arshad, M., Rafique, M., Barakat, M.A. (2019). Butterfly cluster like lamellar BiOBr/TiO_2 nanocomposite for enhanced sunlight photocatalytic mineralization of aqueous ciprofloxacin. Science of the Total Environment, 665: 668-677. https://doi.org/10.1016/j.scitotenv.2019.02.145

[163] Fu, S., Yuan, W., Liu, X., et al. (2020). A novel 0D/2D WS_2/BiOBr heterostructure with rich oxygen vacancies for enhanced broad-spectrum photocatalytic performance. Journal of Colloid and Interface Science, 569: 150-163. https://doi.org/10.1016/j.jcis.2020.02.077

[164] Yin, S., Chen, Y., Hu, Q., Li, M., Ding, Y., Shao, Y., Di, J., Xia, J., Li, H. (2019). In-situ preparation of iron (II) phthalocyanine modified bismuth oxybromide with enhanced visible-light photocatalytic activity and mechanism insight. Colloids and Surfaces A: Physicochemical and Engineering Aspects, 575: 336-345. https://doi.org/10.1016/j.colsurfa.2019.05.028

[165] He, M., Zhao, D., Xia, J., Xu, L., Di, J., Xu, H., Yin, S., Li, H. (2015). Significant improvement of photocatalytic activity of porous graphitic-carbon nitride/bismuth oxybromide microspheres synthesized in an ionic liquid by microwave-assisted processing. Materials Science in Semiconductor Processing, 32: 117-124. https://doi.org/10.1016/j.mssp.2014.12.032

[166] Ling, Y., Dai, Y. (2020). Direct Z-scheme hierarchical WO_3/BiOBr with enhanced photocatalytic degradation performance under visible light. Applied Surface Science, 509: 145201. https://doi.org/10.1016/j.apsusc.2019.145201

[167] Wen, X.J., Zhang, C., Niu, C.G., et al. (2016). Facile synthesis of a visible light α-Fe_2O_3/BiOBr composite with high photocatalytic performance. RSC Advances, 6(5): 4035-4042. https://doi.org/10.1039/C5RA21359B

[168] Fu, J., Tian, Y., Chang, B., Xi, F., Dong, X. (2012). BiOBr–carbon nitride heterojunctions: Synthesis, enhanced activity and photocatalytic mechanism. Journal of Materials Chemistry, 22(39): 21159-21166. https://doi.org/10.1039/C2JM34778D

[169] Shenawi-Khalil, S., Uvarov, V., Fronton, S., Popov, I., Sasson, Y. (2012). A novel heterojunction BiOBr/bismuth oxyhydrate photocatalyst with highly enhanced visible light photocatalytic properties. The Journal of Physical Chemistry C, 116(20): 11004-11012. https://doi.org/10.1021/jp3009964

[170] Cui, W., An, W., Liu, L., Hu, J., Liang, Y. (2014). Synthesis of CdS/BiOBr composite and its enhanced photocatalytic degradation for Rhodamine B. Applied Surface Science, 319: 298-305. https://doi.org/10.1016/j.apsusc.2014.05.179

[171] Wu, D., Ye, L., Yue, S., Wang, B., Wang, W., Yip, H.Y., Wong, P.K. (2016). Alkali-induced in situ fabrication of Bi_2O_4-decorated BiOBr nanosheets with excellent photocatalytic performance. The Journal of Physical Chemistry C, 120(14): 7715-7727. https://doi.org/10.1021/acs.jpcc.6b02365

[172] Cao, Q.W., Cui, X., Zheng, Y.F., Song, X.C. (2016). A novel $CdWO_4$/BiOBr p–n heterojunction as visible light photocatalyst. Journal of Alloys and Compounds, 670: 12-17. https://doi.org/10.1016/j.jallcom.2016.02.061

[173] Wang, X.J., Yang, W. Y., Li, F.T., Zhao, J., Liu, R.H., Liu, S.J., Li, B. (2015). Construction of amorphous TiO_2/BiOBr heterojunctions via facets coupling for enhanced photocatalytic activity. Journal of Hazardous Materials, 292: 126-136. https://doi.org/10.1016/j.jhazmat.2015.03.030

[174] Wang, Z., Wang, K., Li, Y., Jiang, L., Zhang, G. (2019). Novel $BiSbO_4$/BiOBr nanoarchitecture with enhanced visible-light driven photocatalytic performance: Oxygen-induced pathway of activation and mechanism unveiling. Applied Surface Science, 498: 143850. https://doi.org/10.1016/j.apsusc.2019.143850

[175] Tu, X., Luo, S., Chen, G., Li, J. (2012). One-pot synthesis, characterization, and enhanced photocatalytic activity of a BiOBr-graphene composite. Chemistry-A European Journal, 18(45): 14359-14366. https://doi.org/10.1002/chem.201200892

[176] Zhang, J., Lv, J., Dai, K., Liang, C., Liu, Q. (2018). One-step growth of nanosheet-assembled BiOCl/BiOBr microspheres for highly efficient visible photocatalytic performance. Applied Surface Science, 430: 639-646. https://doi.org/10.1016/j.apsusc.2017.02.101

[177] Wei, X.X., Cui, H., Guo, S., Zhao, L., Li, W. (2013). Hybrid BiOBr–TiO_2 nanocomposites with high visible light photocatalytic activity for water treatment. Journal of Hazardous Materials, 263: 650-658.

[178] Hu, T., Yang, Y., Dai, K., Zhang, J., Liang, C. (2018). A novel Z-scheme Bi_2MoO_6/BiOBr photocatalyst for enhanced photocatalytic activity under visible light irradiation. Applied Surface Science, 456: 473-481. https://doi.org/10.1016/j.apsusc.2018.06.186

[179] Cui, W., An, W., Liu, L., Hu, J., Liang, Y. (2014). Novel Cu_2O quantum dots coupled flower-like BiOBr for

enhanced photocatalytic degradation of organic contaminant. Journal of Hazardous Materials, 280: 417-427. https://doi.org/10.1016/j.jhazmat.2014.08.032

[180] Gao, J., Gao, Y., Sui, Z., Dong, Z., Wang, S., Zou, D. (2018). Hydrothermal synthesis of BiOBr/$FeWO_4$ composite photocatalysts and their photocatalytic degradation of doxycycline. Journal of Alloys and Compounds, 732: 43-51. https://doi.org/10.1016/j.jallcom.2017.10.092

[181] Guan, S., Yang, H., Sun, X., Xian, T. (2020). Preparation and promising application of novel $LaFeO_3$/BiOBr heterojunction photocatalysts for photocatalytic and photo-Fenton removal of dyes. Optical Materials, 100: 109644. https://doi.org/10.1016/j.optmat.2019.109644

[182] Li, X., Xiong, J., Gao, X., Ma, J., Chen, Z., Kang, B., Liu, J., Li, H., Feng, Z., Huang, J. (2020). Novel BP/BiOBr S-scheme nano-heterojunction for enhanced visible-light photocatalytic tetracycline removal and oxygen evolution activity. Journal of Hazardous Materials, 387: 121690. https://doi.org/10.1016/j.jhazmat.2019.121690

[183] Han, A., Zhang, H., Lu, D., Sun, J., Chuah, G.K., Jaenicke, S. (2018). Efficient photodegradation of chlorophenols by BiOBr/$NaBiO_3$ heterojunctioned composites under visible light. Journal of Hazardous Materials, 341: 83-92. https://doi.org/10.1016/j.jhazmat.2017.07.031

[184] Ao, Y., Wang, K., Wang, P., Wang, C., Hou, J. (2016). Synthesis of novel 2D-2D pn heterojunction BiOBr/La2Ti_2O_7 composite photocatalyst with enhanced photocatalytic performance under both UV and visible light irradiation. Applied Catalysis B: Environmental, 194: 157-168. https://doi.org/10.1016/j.apcatb.2016.04.050

[185] Sabit, D.A., Ebrahim, S.E., Jabbar, Z.H. (2023). Immobilization of 0D CuO/$ZnFe_2O_4$ nanoparticles onto 2D BiOBr nanoplates as dual S-scheme heterostructure for boosting photocatalytic oxidation of levofloxacin in wastewater: Magnetic reusability and mechanism insights. Journal of Photochemistry and Photobiology A: Chemistry, 443: 114849. https://doi.org/10.1016/j.jphotochem.2023.114849

[186] Liu, H., Du, C., Li, M., Zhang, S., Bai, H., Yang, L., Zhang, S. (2018). One-pot hydrothermal synthesis of SnO_2/BiOBr heterojunction photocatalysts for the efficient degradation of organic pollutants under visible light. ACS Applied Materials & Interfaces, 10(34): 28686-28694. https://doi.org/10.1021/acsami.8b09617

[187] Li, W., Zhang, Y., Bu, Y., Chen, Z. (2016). One-pot synthesis of the $BiVO_4$/BiOBr heterojunction composite for enhanced photocatalytic performance. Journal of Alloys and Compounds, 680: 677-684. https://doi.org/10.1016/j.jallcom.2016.04.202

[188] Zhang, L., Yue, X., Liu, J., Feng, J., Zhang, X., Zhang, C., Li, Fan, C. (2020). Facile synthesis of Bi_5O_7Br/BiOBr 2D/3D heterojunction as efficient visible-light-driven photocatalyst for pharmaceutical organic degradation. Separation and Purification Technology, 231: 115917. https://doi.org/10.1016/j.seppur.2019.115917

[189] Liu, Z., Wang, H., Pan, G., Niu, J., Feng, P. (2017). Facile synthesis, structure and enhanced photocatalytic activity of novel BiOBr/Bi (C_2O_4) OH composite photocatalysts. Journal of Colloid and Interface Science, 486: 8-15. https://doi.org/10.1016/j.jcis.2016.09.052

[190] Wang, L., Min, X., Sui, X., Chen, J., Wang, Y. (2020). Facile construction of novel BiOBr/$Bi1_2O_{17}C_{l2}$ heterojunction composites with enhanced photocatalytic performance. Journal of Colloid and Interface Science, 560: 21-33. https://doi.org/10.1016/j.jcis.2019.10.048

[191] Xu, J., Wang, Y., Niu, J., Chen, M. (2019). Facile construction of BiOBr/BiOCOOH pn heterojunction photocatalysts with improved visible-light-driven photocatalytic performance. Separation and Purification Technology, 225: 24-32. https://doi.org/10.1016/j.seppur.2019.05.022

[192] Wen, X.J., Zhang, C., Niu, C.G., Zhang, L., Zeng, G.M., Zhang, X.G. (2017). Highly enhanced visible light photocatalytic activity of CeO_2 through fabricating a novel p–n junction BiOBr/CeO_2. Catalysis Communications, 90: 51-55. https://doi.org/10.1016/j.catcom.2016.11.018

[193] Geng, Y., Li, N., Ma, J., Sun, Z. (2017). Preparation, characterization and photocatalytic properties of BiOBr/ZnO composites. Journal of Energy Chemistry, 26(3): 416-421. https://doi.org/10.1016/j.jechem.2017.01.002

[194] Yan, S., Yang, J., Li, Y., Jia, X., Song, H. (2020). One-step synthesis of ZnS/BiOBr photocatalyst to enhance photodegradation of tetracycline under full spectral irradiation. Materials Letters, 276: 128232. https://doi.org/10.1016/j.matlet.2020.128232

[195] Hu, X., Cheng, L., Li, G. (2017). One-pot hydrothermal fabrication of basic bismuth nitrate/BiOBr composite with enhanced photocatalytic activity. Materials Letters, 203: 77-80. https://doi.org/10.1016/j.matlet.2017.05.123

[196] Tang, Q.Y., Yang, M.J., Yang, S.Y., Xu, Y.H. (2021). Enhanced photocatalytic degradation of glyphosate over 2D CoS/BiOBr heterojunctions under visible light irradiation. Journal of Hazardous Materials, 407: 124798. https://doi.org/10.1016/j.jhazmat.2020.124798

[197] Jia, K. L., Zhu, Z.S., Qu, J., Jing, Y. Q., Yu, X. J., Abdelkrim, Y., Hao, S.M., Yu, Z.Z. (2020). BiOBr/Ag6Si2O7 heterojunctions for enhancing visible light catalytic degradation performances with a sequential selectivity enabled by dual synergistic effects. Journal of Colloid and Interface Science, 561: 396-407. https://doi.org/10.1016/j.jcis.2019.11.005

[198] Song, X.C., Li, W.T., Huang, W.Z., Zhou, H., Zheng, Y.F., Yin, H.Y. (2015). A novel p–n heterojunction BiOBr/$ZnWO_4$: Preparation and its improved visible light photocatalytic activity. Materials Chemistry and Physics, 160: 251-256. https://doi.org/10.1016/j.matchemphys.2015.04.033

[199] Hu, M., Yan, A., Huang, J., Huang, F., Li, F., Cui, Q., Li, Q., Wang, X. (2019). Novel 2D hybrids composed of $SnIn_4S_8$ nanoplates on BiOBr nanosheets for enhanced photocatalytic applications. Nanotechnology, 31(10): 105202. https://doi.org/10.1088/1361-6528/ab5a1f

[200] Zhao, H.J., Wu, R J., Wang, X.C., An, Y.M., Zhao, W.X., Ma, F. (2020). Heterojunction of $BiPO_4$/BiOBr photocatalysts for Rhodamine B dye degradation under visible LED light irradiation. Journal of the Chinese Chemical Society, 67(6): 1016-1023. https://doi.org/10.1002/jccs.201900344

[201] Sin, J.C., Lam, S.M., Zeng, H., Lin, H., Li, H., Kumaresan, A.K., Mohamed, A.R., Lim, J.W. (2020). Z-

scheme heterojunction nanocomposite fabricated by decorating magnetic $MnFe_2O_4$ nanoparticles on BiOBr nanosheets for enhanced visible light photocatalytic degradation of 2, 4-dichlorophenoxyacetic acid and Rhodamine B. Separation and Purification Technology, 250: 117186. https://doi.org/10.1016/j.seppur.2020.117186

[202] Chen, J., Yang, Q., Zhong, J., Li, J., Burda, C. (2021). Microwave-assisted preparation of flower-like C_{60}/BiOBr with significantly enhanced visible-light photocatalytic performance. Applied Surface Science, 540: 148340. https://doi.org/10.1016/j.apsusc.2020.148340

[203] Hu, M., Yan, A., Cui, Q., Huang, F., Li, D., Li, F., Huang, J., Qiang, Y.H. (2020). NiS/BiOBr hybrids with retarded carrier recombination and enhanced visible-light-driven photocatalytic activity. Journal of Materials Science, 55: 4265-4278. https://doi.org/10.1007/s10853-019-04288-9

[204] Chowdhury, A.P., Shambharkar, B.H. (2020). Fabrication and characterization of BiOBr-$SnWO_4$ heterojunction nanocomposites with boosted photodegradation capability. Chemical Engineering Journal Advances, 4: 100040. https://doi.org/10.1016/j.ceja.2020.100040

[205] Zhang, Z., Ge, X., Zhang, X., Duan, L., Li, X., Yang, Y., Lü, W. (2018). A sea cucumber-like BiOBr nanosheet/Zn_2GeO_4 nanorod heterostructure for enhanced visible light driven photocatalytic activity. Materials Research Express, 5(1): 015009. https://doi.org/10.1088/2053-1591/aa9fc7

[206] Cao, J., Xu, B., Luo, B., Lin, H., Chen, S. (2011). Novel BiOI/BiOBr heterojunction photocatalysts with enhanced visible light photocatalytic properties. Catalysis Communications, 13(1): 63-68. https://doi.org/10.1016/j.catcom.2011.06.019

[207] Obregón, S., Mendoza-Reséndez, R., Luna, C. (2017). Facile synthesis of ultrafine akaganeite nanoparticles for the removal of hexavalent chromium: Adsorption properties, isotherm and kinetics. Journal of Nanoscience and Nanotechnology, 17(7): 4471-4479. https://doi.org/10.1166/jnn.2017.14198

[208] Fang, Y.F., Li, X.Y., Jia, M.K., Huang, Y.P. (2014). Photodegradation of Microcystine-LR uising BiOBr under UV and visible light irradiation. Applied Mechanics and Materials, 488: 248-251. https://doi.org/10.4028/www.scientific.net/AMM.488-489.248

[209] Wang, L.L., Ma, W.H., Wang, S.L., Zhang, Y., Jia, M.K., Li, R.P., Zhang, A.Q., Huang, Y.P. (2012). The contrastive research in the photocatalytic activity of BiOBr synthesized by different reactants. Journal of Nanomaterials, 2012: 619761. https://doi.org/10.1155/2012/619761

[210] Ahmad, A., Meng, X., Yun, N., Zhang, Z. (2016). Preparation of hierarchical BiOBr microspheres for visible light-induced photocatalytic detoxification and disinfection. Journal of Nanomaterials, 2016: 1373725. https://doi.org/10.1155/2016/1373725

[211] Chen, S., Yang, F., Cao, Z., Yu, C., Wang, S., Zhong, H. (2020). Enhanced photocatalytic activity of molybdenum disulfide by compositing ZnAl–LDH. Colloids and Surfaces A: Physicochemical and Engineering Aspects, 586: 124140. https://doi.org/10.1016/j.colsurfa.2019.124140

[212] Mozia, S., Tomaszewska, M., Morawski, A.W. (2005). Photocatalytic degradation of azo-dye Acid Red 18. Desalination, 185(1-3): 449-456. https://doi.org/10.1016/j.desal.2005.04.050

[213] Gondal, M.A., Chang, X., Ali, M.A., Yamani, Z.H., Zhou, Q., Ji, G. (2011). Adsorption and degradation performance of Rhodamine B over BiOBr under monochromatic 532 nm pulsed laser exposure. Applied Catalysis A: General, 397(1-2): 192-200. https://doi.org/10.1016/j.apcata.2011.02.033

[214] Wen, X. J., Niu, C. G., Zhang, L., Liang, C., Zeng, G. M. (2017). An in depth mechanism insight of the degradation of multiple refractory pollutants via a novel $SrTiO_3$/BiOI heterojunction photocatalysts. Journal of Catalysis, 356: 283-299. https://doi.org/10.1016/j.jcat.2017.10.022

[215] Lyu, J., Hu, Z., Li, Z., Ge, M. (2019). Removal of tetracycline by BiOBr microspheres with oxygen vacancies: Combination of adsorption and photocatalysis. Journal of Physics and Chemistry of Solids, 129: 61-70. https://doi.org/10.1016/j.jpcs.2018.12.041

[216] Chen, F., Yang, Q., Li, X., Zeng, G., Wang, D., Niu, C., Zhao, J.W., An, H.X., Xie, T., Deng, Y. (2017). Hierarchical assembly of graphene-bridged Ag_3PO_4/Ag/$BiVO_4$ (040) Z-scheme photocatalyst: an efficient, sustainable and heterogeneous catalyst with enhanced visible-light photoactivity towards tetracycline degradation under visible light irradiation. Applied Catalysis B: Environmental, 200: 330-342. https://doi.org/10.1016/j.apcatb.2016.07.021

[217] Wei, Z., Li, R., Wang, R. (2018). Enhanced visible light photocatalytic activity of BiOBr by in situ reactable ionic liquid modification for pollutant degradation. RSC advances, 8(15): 7956-7962. https://doi.org/10.1039/C7RA13779F

[218] Li, J., Sun, S., Qian, C., He, L., Chen, K. K., Zhang, T., Chen, Z.L., Ye, M. (2016). The role of adsorption in photocatalytic degradation of ibuprofen under visible light irradiation by BiOBr microspheres. Chemical Engineering Journal, 297: 139-147. https://doi.org/10.1016/j.cej.2016.03.145